The 1923 Kanto Earthquake Re-evaluated Using a Newly Augmented Geodetic Data Set.

M. Nyst,[1,2] T. Nishimura,[3] F. F. Pollitz,[1] and W. Thatcher[1]

M. Nyst, Department of Geophysics, Stanford University, Stanford, USA. (mnyst@pangea.stanford.edu)

[1]U. S. Geological Survey, Menlo Park, USA

[2]Now at Department of Geophysics, Stanford University, Stanford, USA

[3]Geographical Survey Institute, Tsukuba, Japan.

Abstract. This study revisits the mechanism of the 1923 M_s=7.9 Kanto earthquake in Japan. We derive a new source model and use it to assess quantitative and qualitative aspects of the release of accumulated plate motion in the Kanto region. We use a new geodetic data set that consists of displacements from leveling and angle changes from triangulation measurements obtained in surveys between 1883 and 1927. Two unique aspects of our analysis are the inclusion of a large number of second order triangulation measurements and the application of a correction to remove interseismic deformation. The geometry of the fault planes is adopted from a recent seismic reflection study of the Kanto region. We evaluate the minimum complexity necessary in the model to fit the data optimally. Our final uniform-slip elastic dislocation model consists of two adjacent ≈20° dipping low-angle planes accommodating reverse dextral slip of 6.0 m on the larger, eastern plane and 9.5 m on the smaller, western plane with azimuths of 163° and 121°, respectively. The earthquake was located in the Sagami trough, where the Philippine Sea plate subducts under Honshu. Compared to the highly oblique angle of plate convergence the coseismic slip on the large fault plane has a more orthogonal orientation to the strike of the plate boundary, suggesting that slip partitioning plays a role in accommodation of plate motion. What other structure is involved in the partitioning is unclear. Uplift records of marine coastal terraces in Sagami Bay document 7,500 years of earthquake activity and predict average recurrence intervals of 400 years for events with similar vertical displacement profiles as the 1923 earthquake. This means that

the average slip deficit per recurrence interval is about 50% of the relative plate convergence. These findings of plate motion partitioning and slip deficit lead us to suggest that, instead of a simple recurrence model with characteristic earthquakes, additional mechanisms are necessary to describe the accommodation of deformation in the Kanto region. So far, obvious candidates for these alternative mechanisms have not been discovered.

1. Introduction

The $M_s = 7.9$ 1923 Kanto earthquake was one of the most destructive events of the 20th century, causing the deaths of over 140,000 people and destroying Yokohama and large parts of Tokyo. Today, the Tokyo metropolitan area houses more than 30 million people. It accounts for a third of Japan's economy and dominates politics, trade, finance, arts and communication. It is not difficult to imagine that a similar earthquake today would not only cause a human tragedy of immeasurable proportions, but would also have catastrophic effects on the Japanese and world economies. In this paper we adopt a source model that optimally fits a set of geodetic measurements of coseismic deformation. To assess the seismic hazard of the Tokyo Bay region, such a model plays a crucial role. First, it has important implications for the derivation of recurrence times of similar earthquakes that may be characteristic for this area [*Thatcher,* 1990]. Furthermore, it provides a basis for calculating the changes in the static stress field caused by the earthquake and its aftereffects that may have influenced subsequent seismicity [*Harris*, 1998; *Toda et al.* 1998]. In an accompanying paper [*Nyst et al.,* 2004] we address the coseismic stress changes computed with the source model presented here.

The tectonic setting of the Tokyo Bay area is complex. The earthquake's epicenter has been located in the Sagami trough [*Ando,* 1971; *Kanamori,* 1971], where the Philippine Sea plate subducts in northwestward direction at an highly oblique angle to the boundary with overriding northern Honshu [*Seno et al.*, 1993, 1996; *Heki et al.*, 1999] (Figure 1A). The westward directed convergence of the Pacific plate with respect to northern Honshu is accommodated by subduction of the Pacific plate along the Japan trench. Collision of the Izu arc on the Philippine Sea plate into the Ogasawara arc on Honshu north of Izu Peninsula determines the surface deformation west of the Sagami trough [e.g., *Huchon and Kitazato*, 1984; *Sagiya et al.*, 2000]. The two subducting plates meet below Kanto, where seismicity shows that the younger, more buoyant Philippine Sea plate is located above the Pacific plate [e.g., *Ishida,* 1992; *Noguchi,* 2002] (Figure 1B).

Early studies of the 1923 earthquake by *Kanamori and Miyamura* [1970], *Kanamori* [1971] and *Ando* [1971, 1974] used seismological and geodetic data to show that the earthquake nucleated in the Odawara region and that the main shock consisted of right-lateral slip with a thrust component on a low-angle fault plane in the Sagami trough. Subsequent studies, based on geodetic, seismological or geological observations or some combination of them, modeled the source mechanism in more detail. *Matsu'ura et al.* [1980] inverted geodetic data for one and two segment uniform slip source models (Figure 1C), which were subsequently refined by *Matsu'ura and Iwasaki* [1983]. *Wald and Somerville* [1995] used the fault plane geometry of the single uniform slip fault model of *Matsu'ura et al.* [1980] to invert geodetic and seismic data to obtain a spatially varying slip model, recently updated by *Kobayashi and Koketsu* [2005]. The geometry and location of the 1923 fault plane as they are inferred from uplift records of marine coastal terraces [*Ando,* 1974; *Matsuda et al.*, 1978; *Shishikura*, 2003] roughly agree with the results from geodetic modeling studies.

A recent seismic reflection study by *Sato et al.* [2005] confirms the fault plane to be the upper surface of the Philippine Sea plate. However, the depth to the top of this plate, 4 to 26 kilometers, is shallower than previous estimates based on the distribution of seismicity [e.g., *Ishida*, 1992; *Noguchi*, 2002]. Furthermore, the dip of the imaged fault plane, about 20° or below, is smaller than presented in previous studies. This is illustrated by Figure

1C, where isodepth contours for the Philippine Sea plate according to *Sato et al.* [2005] are plotted together with the fault plane of the model by *Matsu'ura et al.* [1980]. *Sato et al.* [2005] found that, compared to the variable slip models of *Wald and Somerville* [1995] and *Kobayashi and Koketsu* [2005], their shallower plate geometry shifts the location of maximum slip of the 1923 earthquake towards the north, i.e. towards Tokyo.

Like in previous studies based on geodetic data we use observations from leveling and first order triangulation measurements that were obtained in campaigns between 1883 and 1927. Unique aspects of the data set in this study are: (1) the use of angle changes rather than displacements from the triangulation measurements, to avoid some major sources of systematic error; (2) the adjustment of the geodetic data for interseismic deformation; and (3) the inclusion of a large number of second order triangulation data that densely sample the Kanto plain. In the first part of the paper we compare the data fit of existing source models and investigate what level of complexity is needed to explain our set of observations. We adopt the fault plane geometry as imaged by *Sato et al.* [2005] as a priori information and then determine the optimum source model. We do not incorporate seismological observations into our computations, because except for two seismograms recorded in Tokyo, only teleseismic observations are available [*Kanamori,* 1971; *Takeo and Kanamori,* 1992] and these have been shown to be of limited value in modeling the coseismic slip [*Matsu'ura,* 1980; *Wald and Somerville,* 1996; *Kobayashi and Koketsu,* 2005].

2. Geodetic data

The data used in this study consist of triangulation and leveling data obtained during 2 campaign periods, before and shortly after the 1923 earthquake. In the late 19th century the *Military Land Survey* [1930] of Japan established and surveyed the national geodetic network that consists of horizontal first order control points for triangulation and leveling measurements along roads (Figure 2). At the same time a secondary triangulation network was established to enable a denser spatial sampling of the area. The distance between the first order triangulation points ranges between 20 and 100 km, the second order points are separated by about 10 km (Figure 3). The second order sites are surveyed with lower-quality instrumentation and procedures, generally resulting in measurements with larger uncertainties. The first resurveys of these networks were performed in the immediate aftermath of the 1923 earthquake between 1924 and 1931. We exclude geodetic data that were obtained on Izu Peninsula in the first two years after the 1930 $M_s = 7.3$ Kita-Izu earthquake [*Matsuda,* 1972] (Figure 3). Since the surveys, especially the second order triangulation surveys at some sites, span relatively long time intervals of up to 42 years, the geodetic observations include significant interseismic deformation. Under the assumption that the deformation rates before and after the earthquake are similar [*Sagiya and Thatcher,* 1997] we apply corrections using an interseismic deformation model based on continuous GPS measurements made between 1995 and 2000 [*Nishimura and Sagiya,* 2004]. Tables A1 and A2 *in the electronic supplement* list data, data uncertainties determined in sections 2.1 and 2.2 and time span of the measurement, together with the interseismic adjustment computed for each site in section 2.3.

2.1. Triangulation

The initial first order triangulation survey took place between 1891 and 1898. First order post-earthquake surveys were done between 1924 and 1931 [*Military Land Survey,* 1930]. In addition we use the observations from the second order triangulation network that were obtained in a pre-earthquake campaign between 1883 and 1902 and a post-earthquake survey between 1924 and 1925 (Table 1). *Fujii and Nakane* [1983] use this second order triangulation data set in their study of the crustal strain field in Kanto, but it has never been previously used in studying the Kanto earthquake.

Two general approaches exist to use triangulation data for the determination of surface deformation. Previous geodetic studies of the Kanto earthquake are all based on the same method. A reference frame is constructed from several triangulation sites that are assumed to have remained stable during the period of observation. The coordinates of all sites are explicitly determined at each epoch with respect to this reference frame and then displacement vectors are computed from the difference in station position [e.g., *Bibby*, 1981; *Walcott*, 1984]. *Muto* [1932] converted the first order triangulation data into a displacement data set that formed the basis for the early models of *Ando* [1970, 1974]. *Matsu'ura et al.* [1980] show that movement of the reference system defined by *Muto* [1932] causes a systematic error in the displacement field. They removed this artefact by choosing a more stable reference frame. Later models by *Wald and Somerville* [1995] and *Pollitz et al.* [1996] are based on the displacement vector set of *Matsu'ura et al.* [1980]. Another source of error in this method, one that is impossible to remove completely, is the unavoidable propagation through the network of measurement errors at individual stations. We choose to apply an alternative method that uses the difference between repeated angle observations as a measure of relative deformation of the network to avoid reference frame problems and to minimize the influence of systematic errors [*Frank*, 1966; *Savage and Burford*, 1970; *Thatcher*, 1975; *Yu and Segall*, 1996]. A disadvantage of this approach is that we can only use repeated angle observations instead of all measurements.

Figure 3 shows the triangle network in which the angles were observed at least twice. Because none of the angles between Oshima Island and Japan's mainland were repeated before and after 1923 our data set does not contain information on the deformation across Sagami Bay, and the number of first order data used in this study is somewhat smaller than in to previous studies. However, due to the inclusion of second order data the spatial density of our data set is considerably higher. Our final triangulation data set consists of 31 first and 435 second order repeated angle observations. The largest angle changes were measured in the southwestern part of Boso Peninsula, in Miura Peninsula and along the coast of the Odawara region. The first order angle change data clearly represent a coseismic deformation field of NW-SE oriented extension and to a lesser degree shortening in a NE-SW direction. Although the second-order angle changes provide a shorter wavelength mapping of the coseismic deformation, the overall trend shows NW-SE directed extension west of the Tokyo Bay and NNW-SSE to NNE-SSW oriented extension on Boso Peninsula.

In determining the accuracy of the triangulation measurements we use the method of triangle closure [e.g., *Bomford,* 1980; *Yu and Segall*, 1996]. The measurement error or triangle closure is

$$\delta c = \alpha + \beta + \gamma - (180 + \phi_e) \tag{1}$$

where α, β and γ are the three observed angles in a closed triangle and ϕ_e is the spherical excess. The spherical excess is given by $\phi_e = mab \sin C$, with a and b the lengths of the two sides opposite to angles α and β, respectively, C is their included angle and m is a factor which depends on the latitude. Following *Bomford* [1980] an estimate of the average observational error, ϵ_a, in a network with N closures is then:

$$\epsilon_a = \sqrt{\frac{\sum_{i=1}^{N}(\delta c)^2}{3N}} \tag{2}$$

We consider all angle measurements of closed triangles for campaigns between 1883 and 1931 in the area of central Honshu that encompasses the Kanto district. We find that both first and second order closures follow a normal distribution (Figures 4A and B). Furthermore, closures are evenly distributed over the region, i.e. the data sample the region homogeneously, and the size of the triangle closures shows a random spatial distribution, i.e. the size of the data error is independent of location. Therefore, we assume that we can safely adopt a simple average error for the triangulation observations in our modeling calculations. Average observational errors for the first and second order triangulation networks range between 0.79-0.83 and 1.23-1.31 arcsec, respectively (Table 1). The value for the first order network is consistent with the estimate of 0.7-1.2 arcsec by *Sagiya and Thatcher* [1999] for first order angle change observations at the Nankai Trough between about 1890 and 1950. As reported elsewhere [Japan Association of Surveyors, 1970] the average error of the second order data is surprisingly small. Because comparison of the average error before 1923 and after 1923 for first and second order networks shows no large differences, we use 0.82 arcsec for the first order observations and 1.23 arcsec for the second order triangulation observations.

2.2. Leveling data

The leveling measurements were obtained from first order double-run leveling surveys of the 10 routes shown in Figure 5 during two campaign periods. The average length of one first order leveling section is around 2 km long. The pre-earthquake leveling surveys took place between 1891 and 1918. Post-earthquake data were collected between 1923 and 1930 [*Military Land Survey,* 1930] (Table 2).

In double-run surveys the routes are leveled in both directions. Leveling error accumulates with the square root of distance along the route, expressed as $\alpha\sqrt{L}$, where α (in $mm/\sqrt{km}$) is calculated from differences between forward and backward measurements along a first order route and L (in km) is the section length. For first order surveys, if α exceeds a set tolerance, the section must be rerun (see also *Marshall et al.* [1991]). Since 1955, the Geographical Survey Institute (GSI) has officially released a standard annual average for α. Errors in earlier surveys need to be determined on a case-by-case basis, which gives rise to several problems. First, it is extremely time-consuming to input all data for forward and backward measurements and then calculate the measurement errors or circuit misclosures. In addition, some of the original notes are missing and existing notes can be difficult to understand, because of rough handwriting or the poor physical quality of these old field notes. Since the observation method of leveling has not changed very much since its introduction to Japan, we determine the data errors in a pragmatic, approximate way. We divide the time interval between 1880 and 1945 into two periods and determine an average error for each period. The first period is from 1880 to 1923 following the Kanto earthquake. The second is from 1924 to 1945, the end of World War II. We digitize the height differences of forward and backward measurements of a number of random sections measured in the Kanto district (about 350 for the first time period and about 800 for the second period), calculate the differences between forward and backward runs (listed per year in Table 3) and estimate the average value for α per year. The data from 1884 are significantly less precise than the observations obtained in later years.

Since this was the initial first order leveling campaign done in Japan, its lower precision is probably due to a different initial value for the field tolerance β. Because the leveling error remains relatively stable after the 1890s and the oldest data used in this study are from 1891, we exclude the 1884 α-value from our analysis. The lower row of Table 3 lists the formal values for $\tilde{\alpha}$, the average leveling error for each multiple year period, that we adopt here: 0.54 mm for the period before 1923 and 0.62 mm for the years 1923 to 1925. We smooth the leveling data for each route by removing obvious outliers and small-scale ($<$ 10km) deviations from the regional trend in the data. We utilize the tide gage record that shows a coseismic sea level change of 1.39 m at Aburatsubo (Figure 2) to establish an absolute reference frame for the elevation changes. The final leveling data set consists of 469 measurements (Table 2). Since leveling is a very precise technique for measuring surface deformation, its errors are very small compared to the errors of the angle changes in triangulation surveys. This is illustrated by the difference in signal-to-noise ratio of both data types, which is 43.78 for the leveling data and 5.88 for the first and second order triangulation data combined (Table 2).

Figure 5 shows the vertical displacement data obtained along routes I through IX. The locations of strongest vertical deformation coincide with the areas of largest angle changes (section 2.1). The vertical coseismic deformation reveals uplifts of around 1.5 m on route I at the southern part of Boso Peninsula and on route II at the southernmost tip of Miura Peninsula. The maximum uplift of up to 2 m is measured along the coast at Odawara on route III. We omit from the final data set the part of route IV on Izu Peninsula that was measured immediately after the 1930 $M_s = 7.3$ Kita-Izu earthquake [*Matsuda,* 1972] (Figure 3). The region west of Tokyo along route V underwent subsidence with a maximum of 0.5 m. Towards the east in Tokyo and vicinity along routes VI and IX relatively small displacements, predominantly subsidence, were measured.

2.3. Postseismic and Interseismic Deformation

In this study we are most interested in the coseismic signal in the geodetic data set. Some of the individual measurements, however, span time intervals of several decades to a maximum of 40 years. With earthquake repeat times of 200 to 400 years for 1923-type events in the Sagami trough [*Shishikura*, 2003], these data time spans may account for 5 to 20% of the recurrence time. Assuming that the style and rate of interseismic deformation in the Kanto district, averaged over a time interval of the order of decades, are the same before and after the Kanto earthquake, some nominally coseismic observations must then be significantly influenced by interseismic deformation.

To adjust for these influences we integrate the interseismic velocity over the appropriate time interval at each site by using the interseismic model of *Nishimura and Sagiya* [2004] for the Kanto region based on continuous GPS data (Figure 6). The horizontal interseismic velocity field with respect to stable Eurasia is dominated by two effects: (1) the westward motion of the Pacific plate that is resisted by shallow locking along the Japan trench; and (2) the northwestward convergence of the Philippine Sea plate along the Sagami trough (Figure 6A). The southwestern part of Boso Peninsula, Miura Peninsula and the coastal area between Miura and Izu Peninsulas experience subsidence, while the rest of the area shows uplift (Figure 6B). Since the interseismic velocity field is opposite in sense to the coseismic deformation almost everywhere, adjustment of the coseismic data for interseismic deformation causes an overall increase in the coseismic signal. Two reasons cause the adjustment for interseismic deformation to be larger for the angle changes than for the leveling data: First, on average the triangulation observations span longer time intervals and thus have accumulated more interseismic deformation. Second, much of the leveling data is located farther from the interseismically most active region around the subduction zone. For angle changes the average adjustment is about 15% of the original observations, whereas for leveling data it is about 5%.

The postseismic geodetic surveys for both triangulation and leveling that are used in this study were done within 2 years after the 1923 event and postseismic afterslip and perhaps visco-elastic relaxation influence the records (see *Pollitz et al. [2005b]*). We have insufficient knowledge of its pattern and its magnitude to satisfactorily correct the coseismic signal in the geodetic data. However, available observations show that the postseismic deformation, accumulated between 1923 and 1925 is only a minor contaminant in the coseismic data [*Thatcher and Rundle*, 1979] and we make no corrections for it.

3. Existing models

All existing models of the 1923 Kanto earthquake show right-lateral reverse slip and a fault plane location on the interface between the Philippine Sea plate and northern Honshu. However, some detailed features, listed in Table 4, show large variability. Figure 7 shows the projection onto the Earth's surface of fault planes of the studies discussed in this section. To quantitatively analyze the main characteristics of the existing models for the 1923 Kanto earthquake we compute misfits between the geodetic data used in this study and the predicted deformation for each model. To quantify the goodness of fit we use the normalized root-mean square (NRMS) misfit function, defined as

$$\mathrm{MF}_c = \sqrt{\frac{1}{N - dof} \sum_{n=1}^{N} \left(\frac{\sigma_m}{(w_i \sigma_i + \sigma_m)^2} \right)^2} \qquad (3)$$

with N the number of data, dof the number of degrees of freedom, σ_m the modeling error defined by the difference between the ith observation d_i, and the ith prediction p_i, σ_i the standard deviation of d_i, and w a weighting factor. Computation of the NRMS misfit for a data set consisting of both leveling and triangulation data would be dominated by the misfit between model and leveling data due to the high signal-to-noise ratio of the leveling data (Table 2). Introduction of w allows us to consider one data misfit value based on both leveling and triangulation data, without having the leveling data dominate the grid search in the modeling to be discussed in the next section. w_i is chosen as the ratio of the signal-to-noise ratios of leveling and triangulation data, with a value of 7.45 for leveling data (and 1.0 for triangulation data). To understand misfit values in terms of fit to both types of data we compute the misfit for triangulation (MF_T) and leveling (MF_L) data separately and for both data types combined (MF). Figure 8 and Table 4 display the three different misfit values for each of the models discussed next.

The first analysis of the 1923 earthquake mechanism by *Ando* [1971], based on triangulation data only, presented a uniform source model with right-lateral slip and a small reverse component on a low-angle fault plane in the Sagami trough. *Matsu'ura et al.* [1980] and *Matsu'ura and Iwasaki* [1983] inverted triangulation and leveling data for uniform source models with one and two planes. The variable slip model of *Wald and Somerville* [1995] is constrained by the leveling and triangulation data of *Matsu'ura et al.* [1980] and to a lesser extent by teleseismic records. Their fault plane, subdivided into 70 cells, is based on model II of *Matsu'ura et al.* [1980], but has a larger length and width so as to encompass the larger slipped area of the model by *Kanamori* [1971], which is based on seismic data. The distributed slip solution consists of two patches of large fault slip ($\approx$ 6 to 7 meters) on the plate interface that coincide with the location and size of the two rectangular dislocations of the two-plane uniform source model of *Matsu'ura* [1980]. The larger area with maximum slip is located at a depth of 10 km just southwest of the coast of Boso Peninsula and the smaller high slip patch is located at 15 km depth below Odawara. The three-fault model by *Pollitz et al.* [1996] consists of uniform slip sources and proposes an east-west trending active strike-slip fault in the southern tip of Boso, the Boso transform fault. The horizontal displacement data in this model have been adjusted for interseismic deformation. Although orientations for strike and rake vary strongly among the different models, the majority of the models are in relatively close agreement on the orientation of the slip vector (Table 4).

Smaller misfits are found for the series of similar models by *Matsu'ura et al.* [1980] and *Matsu'ura and Iwasaki* [1983] (Figure 8, Table 4). The two-plane model of *Matsu'ura et al.* [1980] (Figure 7), fits the data especially well. As described in section 2.1, *Ando*'s [1971] relatively poor fit to the triangulation data is explained by *Matsu'ura et al.* [1980], who corrected for a reference frame error in the horizontal displacements derived from the triangulation data. Surprisingly, applying the additional degrees of freedom in the models by *Wald and Somerville* [1995] and *Pollitz et al.* [1996] does not result in a significantly better data fit.

4. Uniform source models

4.1. Modeling results

Encouraged by the success of the simple earthquake models described in the previous section, our modeling procedure aims at fitting a uniform slip source model to the geodetic data set. Following *Okada* [1985, 1992] this model describes the earthquake as a uniform dislocation on a rectangular fault plane with horizontal upper and lower boundaries in a isotropic, elastic uniform half-space. We adopt a planar parametrization of the image of the plate interface of *Sato et al.* [2005] as a priori information in our analysis. Since the plate interface bends around Izu Peninsula, our parametrization consists of two planar segments, plane 1 indicates the eastern dislocation, plane 2 refers to the western dislocation (Figure 9). Both planes are separated along a linear zone indicated by the thick grey line in Figure 9, but their upper edges are constrained to be connected and at the same depth.

An unconstrained double dislocation model would consist of 18 model parameters, or 9 parameters per dislocation: strike, dip, width and length of the rupture plane, longitude and latitude of one corner of the fault plane, orientation and magnitude of the slip vector, and buried depth of the upper edge of the fault plane. In our case a priori information prescribes strike and dip of both fault planes. The length of plane 1 depends on the coordinates of the eastern edge of plane 1, since the western edge is predetermined. In addition, the depth of the upper edge of plane 1 depends on the width and dip of plane 1. The location of the eastern edge of plane 2 depends on the dip and width of plane 2 and of the depth of its upper edge, which is assumed to be the same as for plane 1.

Our two-plane dislocation is now defined by 9 model parameters: orientation and magnitude of the slip vectors on both planes, width of plane 1, longitude and latitude of the lower, easternmost corner of plane 1, and length and width of plane 2. The data misfit is computed with equation 3. We perform a systematic forward grid search over large ranges of the 9-dimensional parameter space to find the best-fitting source model. Guided by the parameter values that produce the best data fit, these ranges are narrowed down in subsequent grid searches to find a global minimum in the data misfit value MF_c.

The minimum for MF_c resulting from the grid search is 1.1 for a model with right-lateral reverse slip of almost 6 m (Table 4, Figure ??A). The misfit values for the same model computed for each data type, MF_t for triangulation and MF_l for leveling, are 1.7 and 0.9, respectively. The solution resembles solution III by *Matsu'ura et al.* [1980], the principal differences being a larger slip and a deeper buried fault plane in our model.

Our uniform source model fits the data better than any of the previously published models described in section 3 (Figure 8, Table 4). Despite the relatively good data fit, the results show a strong trade-off between the triangulation data fit and the fit to the leveling data for several model parameters. Triangulation data tend to be fit best by a plane 1 with a length of $\approx$ 60 km that is buried at a depth of almost 17 km, whereas leveling data favor a longer fault plane with a relative shift in location towards the southeast (of $\approx 0.1°$). Furthermore, slip based on triangulation data is significantly smaller on plane 1 (3.5 m) with a smaller strike-slip component (rake = 122°) than slip predicted by leveling data alone (6.0 m with a rake of 138°).

The dashed line in Figure 10 shows the predictions by our model together with the measurements of vertical deformation for the leveling routes, indicated by the colored lines. Only where the vertical interseismic displacements have a visible deviation from zero are they plotted. The modeled uplift on Boso Peninsula along route I is too large by about 25 cm, while the model underestimates the uplift near Odawara along route III and overestimates the subsidence near Miura Peninsula along route II. The predicted subsidence along route V, in the area west of Tokyo, is larger than what is measured. The remaining main characteristics of the leveling data are fit by our optimal model. The largest misfits of the angle change data are located in the areas where the largest horizontal deformation is measured; on the southern part of Boso Peninsula, on Miura Peninsula and along the Odawara coastline. Figures 11A and B show that this simple model fits the first order triangulation data well, while it generally underestimates the second order angle changes. Since this two fault plane model fits the main characteristics of the triangulation and leveling data, we adopt it as our preferred static source model for the 1923 earthquake.

4.2. Influence of a layered Earth

We investigate to what extent the predicted deformation field of our solution in a uniform half-space model differs from that in a more realistic, layered Earth model. We apply the method of *Wang* [1999] and *Wang et al.* [2003] to calculate static coseismic deformation in an isotropic, elastic continuum which consists of an arbitrary but finite number of laterally homogeneous layers, with the deepest layer extending to infinite depth. To represent the crust below Tokyo we use the layered velocity structure obtained by *Takeo and Kanamori* [1992, 1998], listed in Table 5. This structure is derived from a combination of reflection, refraction, borehole and seismic data obtained in the Kanto region.

We compute horizontal and vertical surface deformation with our model in a layered crust and compare the results with those of the uniform half-space model. Overall, we find that the influence of layering is minor and most noticeable in those areas where the strongest coseismic deformation was measured; Boso and Miura Peninsula and Odawara (Figure 12).

Tokyo is located on the Kanto plain, which is covered by soft sedimentary layers with a total thickness of about a kilometer (upper layer in Table 5). These sediments are absent at the southern tips of Boso and Miura Peninsulas, and at western Kanto and Izu Peninsula

[*Sato et al.*, 1998a]. The inclusion of this thin upper layer in ground motion modeling is significant [*Takeo and Kanamori*, 1992, 1997; *Sato et al.*, 1998a, 1998b]. However, it does not influence the static deformation field, since we find no significant differences between deformation computed with and without this top layer.

In addition, we tested two additional layered velocity structure models for Kanto, proposed in independent studies by *Yamazaki et al.* [1992] and *Sato* [1998a, 1998b], with and without soft, sedimentary layers on top. We find that all produce results similar to those obtained using the velocity structure of *Takeo and Kanamori* [1992].

5. Summary and discussion

We use an unprecedented dense historical geodetic data set consisting of triangulation and leveling data that is adjusted for interseismic deformation to model the source mechanism of the 1923 Kanto earthquake in terms of an elastic dislocation. The model that optimally fits the data consists of two adjacent low-angle planes accommodating uniform, reverse dextral slip of 6.0 m and 9.5 m with azimuths of 163° and 121°, respectively. Since the data fit is not sensitive to the application of a layered velocity structure, the preferred source model is defined in a uniform half-space.

5.1. Data fit

Our preferred model fits the data better than any of the previously proposed models with a normalized misfit around 1 (Figure 8).

For the triangulation data the larger normalized misfit of 1.70 is mainly due to the fit of the second order triangulation data (Figure 11a and b): The trend in Figure 11b differs significantly from one. One possible explanation is the uneven distribution of the first-and second order triangulation data over the model area. Figure 2 shows that the first order data hardly record the deformation of the Boso Peninsula, whereas the second order data densely cover this region. The large misfit for the second order data may suggest that our model needs more complexity to correctly represent the coseismic deformation on Boso Peninsula. Furthermore, since the second order data cover on average longer time intervals than the first order data, an incorrect interseismic deformation rate will produce a larger misfit for the second order data.

5.2. Location of the fault plane

The fault planes and isodepth contours of our preferred source model are plotted in Figure 13 together with the isodepth contours of the Philippine Sea plate by *Sato et al.* [2005]. Our model is very similar to model III of *Matsu'ura et al.* [1980] (see Figure 1C). Although the projections of the two models onto the Earth's surface almost completely overlap, our fault planes are shallower due to the lower dipping angle. Also, the western plane accommodates larger slip and has a much shorter width. In general, our smaller fault plane and the western rim of our larger fault plane fit the isodepth contours of the Philippine Sea plate well. The locations of the centers of our two planes coincide with the locations of the two patches of high 1923 coseismic slip in the source model of *Sato et al.* [2005].

According to *Kanamori and Miyamura* [1970], who interpreted seismic observations, the 1923 earthquake nucleated beneath the Odawara region at latitude 35.4°, longitude 139.2° at a depth between 10 and 15 km (star in Figure 13), which coincides with the location of the western fault plane.

5.3. Slip orientation

Azimuths of the coseismic slip vectors in our source model are 163° for the eastern plane and 121° for the western plane (Table 4). Slip on the larger eastern plane is oriented more normal to the strike of the fault plane than is the average relative plate motion orientation (Figure 14). This suggests that along this plane, relative plate motion is partitioned and part of the boundary-parallel plate motion is taken up elsewhere.

As a possible candidate for accommodating the plate-parallel motion, *Lallemant et al.* [1996] and *Pollitz et al.* [1996] propose the Boso Transform fault. According to these authors, this fault is a right-lateral strike-slip fault that surfaces at the southern tips of Boso and Miura Peninsulas. They further propose that it ruptured during the 1923 Kanto earthquake. The surface fault traces are indicated by *b*'s in Figure 13. However, the coseismic triangulation and present-day continuous GPS data do not indicate any significant dextral surface deformation across these fault segments and in other studies these faults are considered to be splay-faults from the subduction plate interface [e.g., *Saito et al.,* 2002]. Therefore, if slip partitioning occurs to make up for the mismatch between the 1923 earthquake slip vector and the expected interplate convergence direction, it is uncertain whether the proposed Boso transform can accommodate the expected right-lateral strike-slip motion.

5.4. Slip magnitude

We compare our 1923 coseismic slip with relative plate motion predicted by plate tectonic models and with a recurrence model derived from uplift records of marine terraces. Subduction of the Pacific plate along the Japan and Izu-Bonin trenches accommodates convergence between the Pacific, northern Honshu and the Philippine Sea plates. The velocity of the Pacific plate with respect to northern Honshu at the latitude of the Sagami trough is about 75 mm/yr in a westward direction [*Seno et al.*, 1996]. The Philippine Sea plate subducts beneath Honshu along the Nankai, Suruga and Sagami troughs. The existing plate motion models predict between 30 mm/yr at an azimuth of 142° [*Sella et al.*, 2002] based on GPS data, 29 mm/yr at an azimuth of 143° [*Seno et al.*, 1993, 1996] based on earthquake slip vectors, and 45 mm/yr at an azimuth of 133° [*Heki et al.*, 1999; *Heki and Miyazaki*, 2001] based on GPS data. For all models, the convergence between the Philippine Sea plate and northern Honshu at the Sagami Trough is highly oblique (Figure 15).

The last big event in the Kanto region before 1923 was the 1703 M_s=8.1 Genroku earthquake. Generally, this event is assumed to have occurred on the interface between the Philippine Sea plate and northern Honshu [*Shishikura,* 2003; *Shishikura et al.,* 2005]. There is a 220 year time interval between the 1923 Kanto earthquake and the Genroku event. Assuming that 100% of the relative plate motion is accommodated by major earthquakes in the Sagami trough, 220 years of accumulating plate motion would result in coseismic slip of 6.6 m at an azimuth of 142° according to *Sella et al.* [2002], 8.6 m at an azimuth of 143° for the model of [*Seno et al.,* 1993, 1996] and 9.9 m at an azimuth of 133° following *Heki et al.* [1999] and *Heki and Miyazaki* [2001]. All these plate models predict higher coseismic slip than the slip predicted by our model on the larger of the two fault planes, overestimating its magnitude by about 10 to 30%.

Uplift records of marine terraces along Boso and Miura Peninsula show a regular pattern of earthquake activity over the past 7,250 years and seem to indicate that two different types of megathrust earthquakes occur on the Sagami Trough [*Matsuda et al.*, 1978;

Shishikura, 2003]. A smaller type of event associated with the 1923 Kanto earthquake causes average uplifts of 1.2 to 1.5 meters every 400 years (± 200 years), while a larger type of event, associated with the M_s=8.1 earthquake that hit Kanto in 1703, causes average uplifts of 3 meters every 2300 years (± 800 years). The vertical displacement caused by the former type of event agrees with our model results. The latter type of event is assumed to rupture over a larger area, extending eastwards from the fault plane derived for the 1923 Kanto earthquake [*Shishikura et al.*, 2005].

Assuming 100% seismic release, convergence rates of 30-45 mm/yr measured by GPS, accumulated over the average recurrence times of 400 years suggested by the marine terrace uplift record, would result in average, characteristic events for the Sagami trough with horizontal coseismic displacements of 12 to 18 m. These slip values require earthquakes that are much larger than the 1923 earthquake. Furthermore, they contradict the moderate height of about 1.2 to 1.5 m of the terraces associated with this 400 year time interval, which can be fit by a 1923-type event (and is predicted by our model).

In summary, several important questions pertaining to the seismic hazard in the Tokyo Bay area remain to be solved. Seismic hazard in the Tokyo Bay area can not be assessed by a simple recurrence model with characteristic earthquakes. Although the 1923 coseismic slip magnitude can be explained by plate motion models of *Seno et al.* [1993, 1996] and *Sella et al.* [2002], the marine terrace record combined with this study's results suggest an alternative mechanism or a combination of mechanisms is responsible for accommodating a slip deficit of up to 50% of the total plate motion across the Sagami trough per average recurrence time interval of 400 years.

Several recent studies propose mechanisms that may resolve some of the problems. The M_s=7.2 1855 Ansei Edo earthquake caused severe damage to Tokyo. Most studies agree on its epicenter being located near Tokyo, while its focal depth and mechanism are debated. Estimated sources include a shallow crustal event, an interplate event on the Philippine Sea Plate-Honshu interface and an intraplate event in the Pacific plate [*Bakun*, 2004 *and references therein*]. Newly interpreted intensity data from the catalogue of *Usami* [1996] best fit a location on either the lower extension of the Philippine Sea plate, the Philippine Sea-Pacific plate interface or the top of the Pacific plate [*Bakun*, 2004]. Based on the abundance of aftershocks recorded of the 1855 earthquake, *Bakun* [2004] locates the event on the lower extension of the Philippine Sea plate at a depth of 30 km, just below the part that ruptured during the 1923 earthquake. If this type of event occurs on a regular basis, it may account for a small part of the accommodation of plate motion, since one can expect the rupture to propagate upwards and release some of the accumulated slip deficit on the plate interface between the surface and 30 km. Unfortunately, the historic earthquake record does not allow for a systematic recognition of Ansei Edo-type events before 1855.

A more promising direction of future research may be the discovery of silent slip events. *Ozawa et al.* [2003] discovered the signal of slow earthquakes on a part of the downgoing slab of the Philippine Sea plate that is located in the Sagami trough southeast of the southern tip of Boso Peninsula. Two silent slip events with an interevent time of 6 years and slip of up to 20 cm were detected. If events like this occur on a regular basis they can account for most or all of the accumulated plate motion predicted by the models of *Sella et al.* [2002], *Seno et al.* [1993, 1996]) and *Heki et al.* [1999]. However, these slip events occurred east of the segments that ruptured during the 1923 event, on which, so far, no evidence has been found for silent slip.

Acknowledgments. We would like to thank Bill Bakun, Tom Parsons, Ross Stein and Shinji Toda for extremely useful discussions during various stages of this research. Thorough reviews by Jim Savage and Jessica Murray improved this manuscript considerably. Suggestions by associate editor Kelin Wang and 2 anonymous reviewers greatly enhanced the structure and readability of the manuscript. We are grateful to Masanobu Shishikura for organizing a field trip to Boso Peninsula and for explaining his work on the dating of the uplift of marine terraces. We acknowledge the help of Mitsuo Ohtaki from GSI in Tsukuba, who computed the errors in the leveling measurements obtained after 1955. Most of the figures in this paper were produced using the public domain GMT software package [*Wessel and Smith*, 1995].

References

Ando, M., A fault-origin model of the Great Kanto earthquake of 1923 as deduced from geodetic data, *Bulletin of the Earthquake Research Institute, 49*, 19–32, 1971.

Ando, M., Seismo-tectonics of the 1923 Kanto earthquake, *J. Phys. Earth, 22*, 263–277, 1974.

Bakun, W. H., Magnitude and location of historical earthquakes in Japan and implications for the 1855 Ansei Edo earthquake, *submitted to J. Geophys. Res.*, 2004.

Bibby, H. M., Unbiased estimate of strain from triangulation data using the method of simultaneous reduction, *Tectonophysics, 82*, 161–174, 1982.

Bomford, G., *Geodesy,* 855 pp., Clarendon, Oxford, 1980.

Frank, F. C., Deduction of earth strains from survey data, *Bull. Seismol. Soc. Am., 56*, 35–42, 1966.

Fujii, Y., and K. Nakane, Horizontal crustal movements in the Kanto-Tokai district, Japan, as deduced from geodetic data, *Tectonophys., 97*, 115–140, 1983.

Harris, R., Introduction to special section: Stress triggers, stress shadows, and implications for seismic hazard, *J. Geophys. Res., 95,* 24,347–24,358, 1998.

Heki, K., S. Miyazaki, H. Takahashi, M. Kasahara, F. Kimata, S. Miura, N. Vasilenko, A. Ivaschenko, and K.-D. An, The Amurian Plate motion and current plate kinematics in eastern Asia, *J. Geophys. Res., 104,* 29,147–29,155, 1999.

Huchon, P., and H. Kitazato, Collision of the Izu block with central Japan during the Quaternary and geological evolution of the Ashigara area, *Tectonophysics, 110,* 201–210, 1984.

Ishibashi, K., Specification of a soon-to-occur seismic faulting in the Tokai district, central Japan, based upon seismotectonics, in *Earthquake Prediction; an International Review,* edited by D. Simpson and P. Richard, pp. 297–332, AGU, Washington, D.C., 1981.

Ishibashi, K., Kanagawaken-Seibu-Earthquake and earthquake prediction I (*in Japanese*), *Kagaku, 58*, 537–547, 1988.

Ishida, M., Geometry and relative motion of the Philippine Sea Plate and Pacific plate beneath the Kanto-Tokai district, Japan, *J. Geophys. Res., 97*, 489–513, 1992.

Ishida, M., and M. Kikuchi, A possible foreshock of a future large earthquake near Odawara, center Japan, *Geophys. Res. Lett., 19*, 1695–1698, 1992.

Heki, K., and S. Miyazaki, Plate convergence and longterm crustal deformation in central Japan, *Geophys. Res. Lett., 28,* 2313-2316, 2001.

Japan Association of Surveyors, History of surveying and mapping for one hundred years *in Japanese*, edited by Editorial Committee for History of Surveying and Mapping for one hundred years, 673 pp., Japan Association of Surveyors, Tokyo, 1970.

Kanamori, H., Faulting of the Great Kanto earthquake of 1923 as revealed by seismological data, *Bull. Earthq. Res. Inst., 49*, 13–18, 1971.

Kanamori, H., and S. Miyamura, Seismometrical re-evaluation of the Great Kanto earthquake of September 1, 1923, *Bull. Earthq. Res. Inst., 48*, 115–125, 1970.

Kobayashi, R., and K. Koketsu, Source process of the 1923 Kanto earthquake inferred from historical geodetic, teleseismic, and strong motion data, *Earth, Planets and Space, 57*, 261–270, 2005

Lallemant, S. J., X. Le Pichon, F. Thoue, P. Henry, and S. Saito, Shear partitioning near the central Japan triple junction: the 1923 great Kanto earthquake revisited - I, *Geophys. J. Int., 126*, 871–881, 1996.

Marshall, G. A., R. S. Stein, and W. Thatcher, Faulting geometry and slip from coseismic elevation changes: The 18 October 1989, Loma Prieta, California, earthquake, *Bull. Seismol. Soc. Am., 81*, 1660–1693, 1991.

Matsuda, T., Surface faults associated with the Kita-Izu earthquake of 1930 in Izu Peninsula, Japan, in *The Izu Peninsula,* edited by M. Oshino and H. Aoki, pp. 77–93, Tokai Univ. Press, Tokyo, 1972.

Matsuda, T., Y. Ota, M. Ando, and N. Yonekura, Fault mechanism and recurrence time of major earthquakes in Southern Kanto district, Japan, as deduced from coastal terrace data, *Geol. Soc. Amer. Bull., 89,* 1610–1628, 1978.

Matsu'ura, M., T. Iwasaki, Y. Suzuki, and R. Sato, Statical and dynamical study on faulting mechanism of the 1923 Kanto earthquake, *J. Phys. Earth, 28*, 119–143, 1980.

Matsu'ura, M., and T. Iwasaki, Study on coseismic and postseismic crustal movements associated with the 1923 Kanto earthquake, *Tectonophys, 97*, 201–215, 1983.

Military Land Survey, Re-survey of the Kwanto district after the great earthquake of 1923, *Bull. Imp. Earthq. Invest. Comm., 11*, 1–6, 1930.

Miyabe, N., On the vertical movement in Kwanto districts, *Bull. Earthq. Res. Inst., Univ. Tokyo, 9,* 1–21, 1931.

Muto, K., A study of the displacements of triangulation points, *Bull. Earthq. Res. Inst., Univ. Tokyo, 10,* 384–392, 1932.

Niitsuma, N., Rupture and delamination of island arc crust due to the arc-arc collision in the South Fossa Magna, central Japan, *The Island Arc, 8*, 441–458, 1999.

Nishimura, T., and T. Sagiya, Crustal block kinematics around the northern Philippine Sea plate, central Japan, estimated from GPS and leveling data, *in preparation*, 2005.

Noguchi, S., Earthquake clusters in the Kanto and Tokai subduction zones: Implications for modes of plate consumption, in *Seismotectonics in Convergent Plate Boundary,* edited by Y. Fujinawa and A. Yoshida, pp. 451–467, TERRAPUB, Tokyo, 2002.

Nyst, M., N. Hamada, F.F. Pollitz, and W. Thatcher, The stress triggering role of the 1923 Great Kanto earthquake, *to be submitted to J. Geophys. Res.*, 2005.

Ohtake, M., A unified seismotectonic model for Kanto and Tokai regions: mechanics of shallow south Kanto earthquakes *in Japanese*, *Bosai-Kagaku-Gijyutsu, (NIED report), 41,* 1–7, 1980.

Okada, Y., Surface deformation due to shear and tensile faults in a half space, *Bull. Seismol. Soc. Am., 75*, 1135–1154, 1985.

Okada, Y., Internal deformation due to shear and tensile faults in a half-space, *Bull. Seis. Soc. Am., 82*, 1018–1040, 1992.

Ozawa, S., S. Miyazaki, Y. Hatanaka, T. Imakiire, M. Kaidzu, M. Murakami, Characteristic silent earthquakes in the eastern part of the Boso peninsula, Central Japan S. Ozawa, *Geophys. Res. Lett., 30*, 1283, 10.1029/2002GL016665, 2003.

Pollitz, F. F., X. Le Pichon and S. J. Lallemant, Shear partitioning near the central Japan triple junction: the 1923 great Kanto earthquake revisited - II, *Geophys. J. Int., 126*, 882–892, 1996.

Pollitz, F. F., M. Nyst, and W. Thatcher, Coseismic slip distribution of the 1923 Kanto earthquake, Part II, *to be submitted to J. Geophys. Res.,* 2005a.

Pollitz, F. F., M. Nyst, and W. Thatcher, Inference of postseismic deformation mechanisms following the 1923 Kanto earthquake, *to be submitted to J. Geophys. Res.,* 2005b.

Sagiya, T., and W. Thatcher, Coseismic slip resolution along a plate boundary megathrust: The Nankai Through, southwest Japan, *J. Geophys. Res., 104*, 1111–1129, 1999.

Sagiya, T., S. Myazaki and T. Tada, Continuous GPS array and present-day crustal deformation of Japan, *Pure Appl. Geophys., 157*, 2303–2322, 2000.

Saito, T., and M. Ito, Deposition of sheet-like turbidite packets and migration of channel-overbank systems on a sandy submarine fan: an example from the Late Miocene-Early Pliocene forearc basin, Boso Peninsula, Japan , *Sedimetary Geology, 149*, 265–277, 2002.

Sato, T., D. V. Helmberger, P. G. Somerville, R. W. Graves and C. K. Saikia, Estimates of regional and local strong motions during the Great 1923 Kanto, Japan, Earthquake (*Ms*

8.2). Part 1: Source estimation of a calibration event and modeling of wave propagation paths, *Bull. Seismol. Soc. Am., 88,* 183–205, 1998a.

Sato, T., R. W. Graves, P. G. Somerville, and S. Kataoka, Estimates of regional and local strong motions during the Great 1923 Kanto, Japan, earthquake (*Ms* 8.2). Part 2: Forward simulation of seismograms using variable-slip rupture models and estimation of near-fault long-period ground motions, *Bull. Seismol. Soc. Am., 88,* 206–227, 1998b.

Sato, H., N. Hirata, K. Koketsu, D. Okaya., S. Abe, R. Kobayashi, M. Matsubara, T. Iwasaki, T. Ito, T. Ikawa, T. Kawanaka, K. Kasahara, S. Harder, Earthquake Source Fault Beneath Tokyo, *Science, 309*, 462–464 , 2005.

Savage, J. C., and R. O. Burford, Accumulation of tectonic strain in California, *Bull. Seismol. Soc. Am., 60*, 1877–1896, 1970.

Sella, G. F., T. H. Dixon, and A. Mao, REVEL: A model for Recent plate velocities from space geodesy, *J. Gephys. Res., 107,* 10.1029/2000JB000033, 2002.

Seno, T., S. Stein, and A. E. Gripp, A model for the motion of the Philippine Sea plate consistent with NUVEL-1 and geological data, *J. Geophys. Res., 98,* 17941–17948, 1993.

Seno, T., T. Sakura, and S. Stein, Can the Okhotsk plate be discriminated form the North American plate? *J. Geophys. Res., 101,* 11,305–11,315, 1996.

Shishikura, M., Cycle of Interplate Earthquake Along the Sagami Trough, Deduced from Tectonic Geomorphology, *Bull. Earthq. Res. Inst. Univ. Tokyo, 78,* 245–254, 2003.

Shishikura, M., S. Toda, and K. Satake, Fault model of the 1703 Genroku Kanto Earthquake (M=8.2) along the Sagami Trough deduced from renewed coseismic crustal deformation, *in preparation*, 2005.

Takeo, M., and H. Kanamori, Simulation of long-period ground motions for the 1923 Kanto earthquake (M = 8), *Bull. Earthquake Res. Inst. Tokyo Univ., 67,* 389–436, 1992.

Takeo, M., and H. Kanamori, Simulation of Long-Period Ground Motion near a Large Earthquake, *Bull. Seismol. Soc. Am., 87,* 140–156, 1997.

Thatcher, W., Strain accumulation and release mechanism of the 1906 earthquake, *J. Geophys. Res., 80*, 4862–4872, 1975.

Thatcher, W., and J.B. Rundle, A model for the earthquake cycle in underthrust zones, *J. Geophys. Res., 84,* 5540-5556, 1979.

Thatcher, W., Order and diversity in the modes of circum-Pacific earthquake recurrence, *J. Geophys. Res., 95,* 2609–2623, 1990.

Toda, S., R. S. Stein, P. A. Reasenberg, J. H. Dieterich, and A. Yoshida, Stress transferred by the 1995 $M_w = 6.9$ Kobe, Japan, shock: Effects on aftershocks and future earthquake probabilities, *J. Geophys. Res., 95,* 24,543–24,566, 1998.

Tsukahara, H., and R. Ikeda, Hydraulic fracturing stress measurements and in-situ stress field in the Kanto-Tokai area, Japan, *Tectonophysics, 135,* 329–345, 1987.

Usami, T., Materials for comprehensive list of destructive earthquake in Japan (*in Japanese*), *Univ. of Tokyo Press*, 1996.

Walcott, R. I., The kinematics of the plate boundary zone through New Zealand: A comparison of short and longterm deformations, *Geophys. J. R. Astron. Soc., 79*, 613–633, 1984.

Wald, D. J., and P. G. Somerville, Variable-slip rupture model of the great 1923 Kanto, Japan, earthquake: Geodetic and body-waveform analysis, *Bull. seismol. Soc. Am., 85*, 159–177, 1995.

Wang, R., A simple orthonormalization method for the stable and efficient computation of Green's functions, Bull. Seism. Soc. Am., 89, 733–741, 1999.

Wang, R., F. Lorenzo, and F. Roth, Computation of deformation induced by earthquakes in a multi-layered elastic crust – FORTRAN programs EDGRN/EDCMP, *Computers and Geosciences, 29*, 195–207, 2003.

Wessel, P., and W. H. F. Smith, New, improved version of the Generic Mapping Tools Released, *EOS Trans. AGU, 79,*, 579, 1998.

Yamanaka, H., Analysis and modeling of long-period ground motion in the Kanto plain, Japan, *Proc. of the 4th International Conference Seismic Zonation,* 75–82, 1991.

Yamazaki, K., M. Minamishima, and K. Kudo, Propagation characteristics of intermediate-period (1-10seconds) surface waves in the Kanto Plain, Japan, *J. Phys. Earth, 40,* 117–136, 1992.

Yu, E., and P. Segall, Slip in the 1868 Hayward earthquake from the analysis of historical triangulation data, *J. Geophys. Res., 101,* 16,101–16,118, 1996.

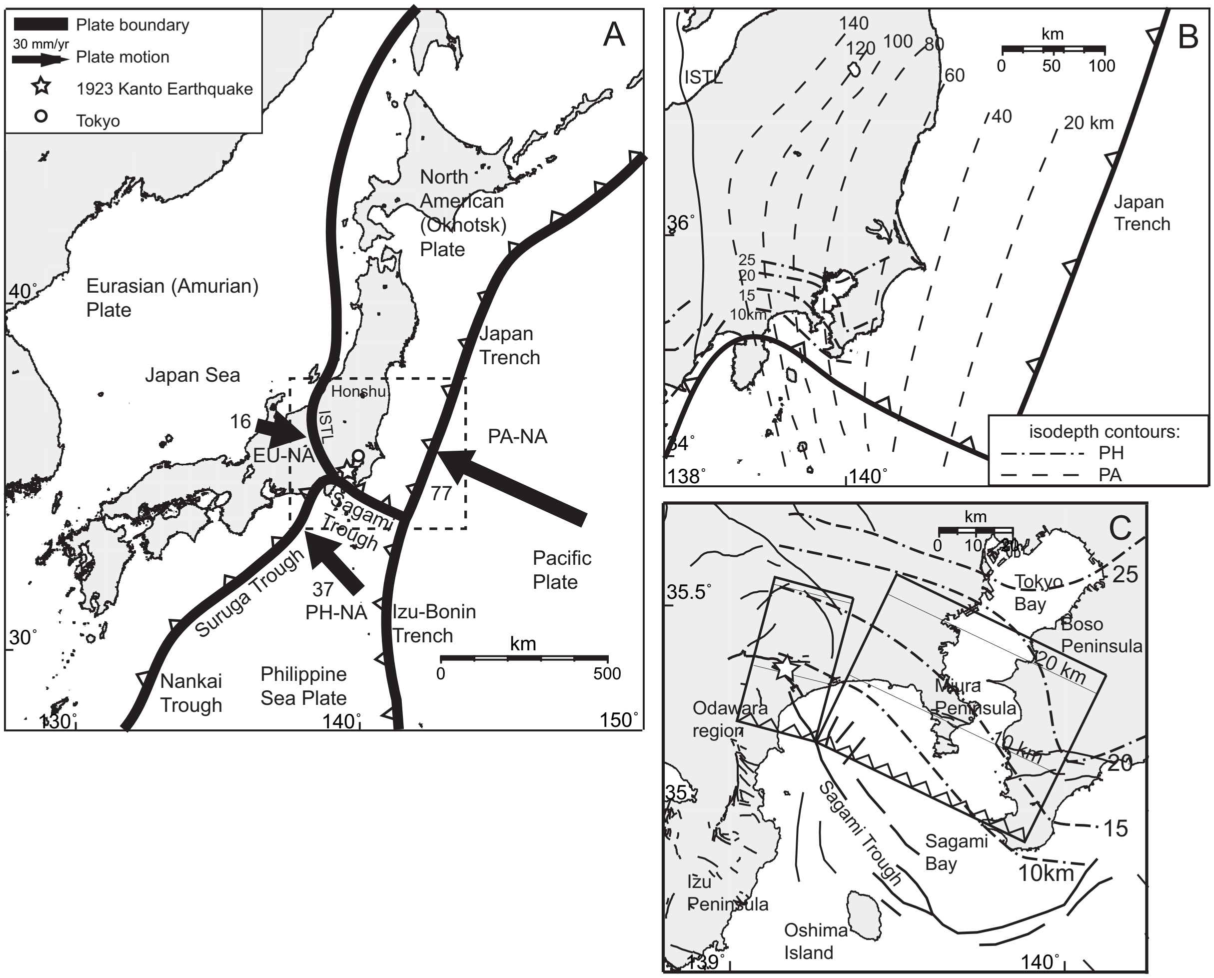

Figure 1. (A) Plate tectonic setting of Japan, where four major plates converge: the Eurasian (EU) or Amurian according to *Heki et al.* [1999] and *Heki and Miyazaki* [2001], North American (NA) or Okhotsk according to *Seno et al.* [1993, 1996], Pacific (PA) and Philippine Sea (PH) plate. Northern Honshu is located on the North American or Okhotsk plate. ISTL Itoigawa-Shizuoka Tectonic Line. The arrows indicate motion of different plates relative to northern Honshu, the numbers are averages of the rate predictions in mm/yr, based on Global Positioning System (GPS) observations [*Heki et al.* 1999, *Seno et al.* 1996]. The dashed square outlines the area shown in (B); (B) Isodepth contours of the surfaces of the PH based on seismic reflection data [from *Sato et al.*, 2005] and the PA plate based on seismicity data [from *Noguchi*, 2002]; (C) Active fault map of the coastal

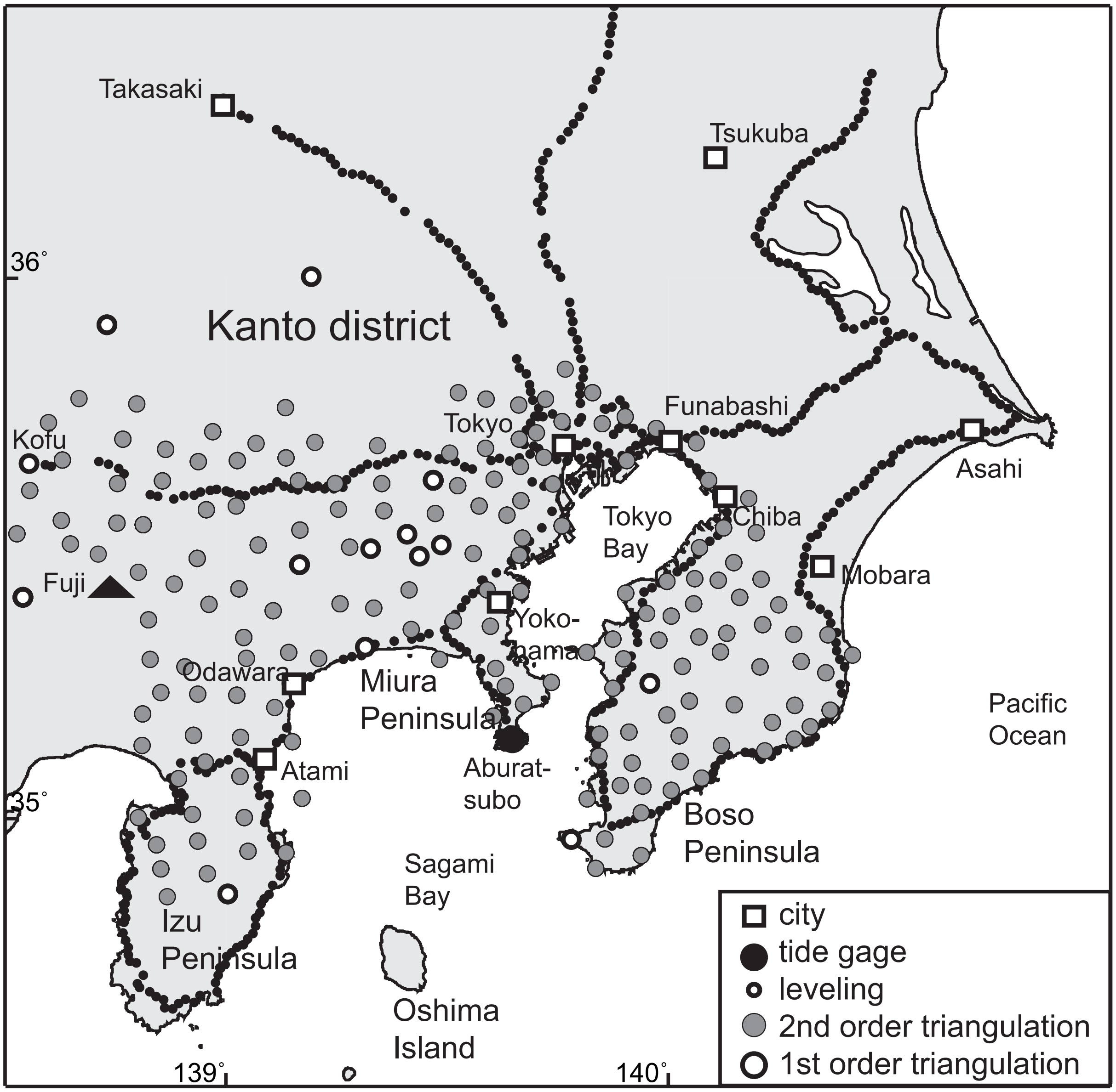

Figure 2. The geodetic observation networks used in this study. The leveling data are tied to an absolute vertical reference frame by using the tide gage records of Aburatsubo station.

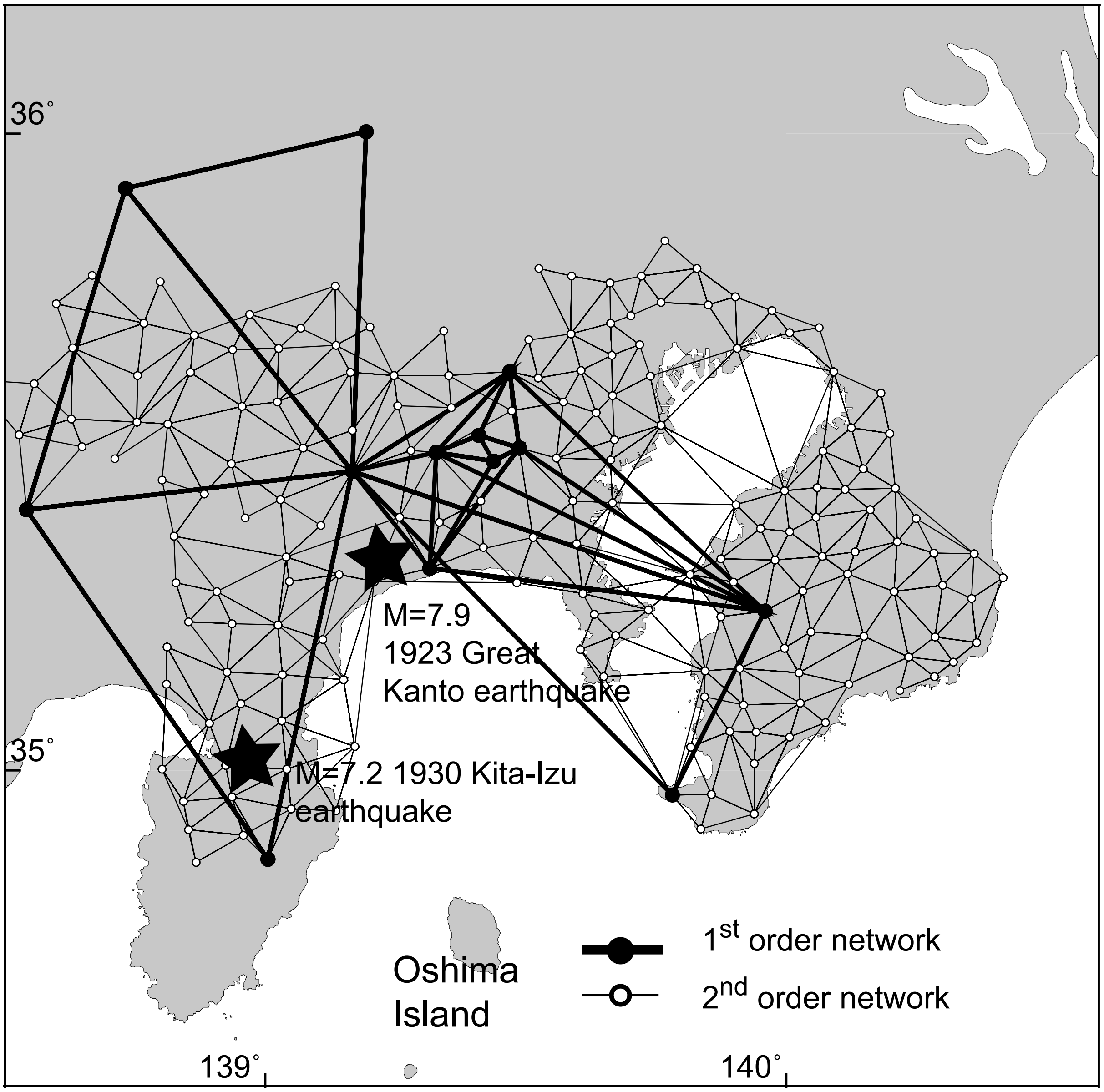

Figure 3. First and second order triangulation networks where repeated angles are available. Stations without repeated angle observations do not contribute to the data set used in this study and are not shown here.

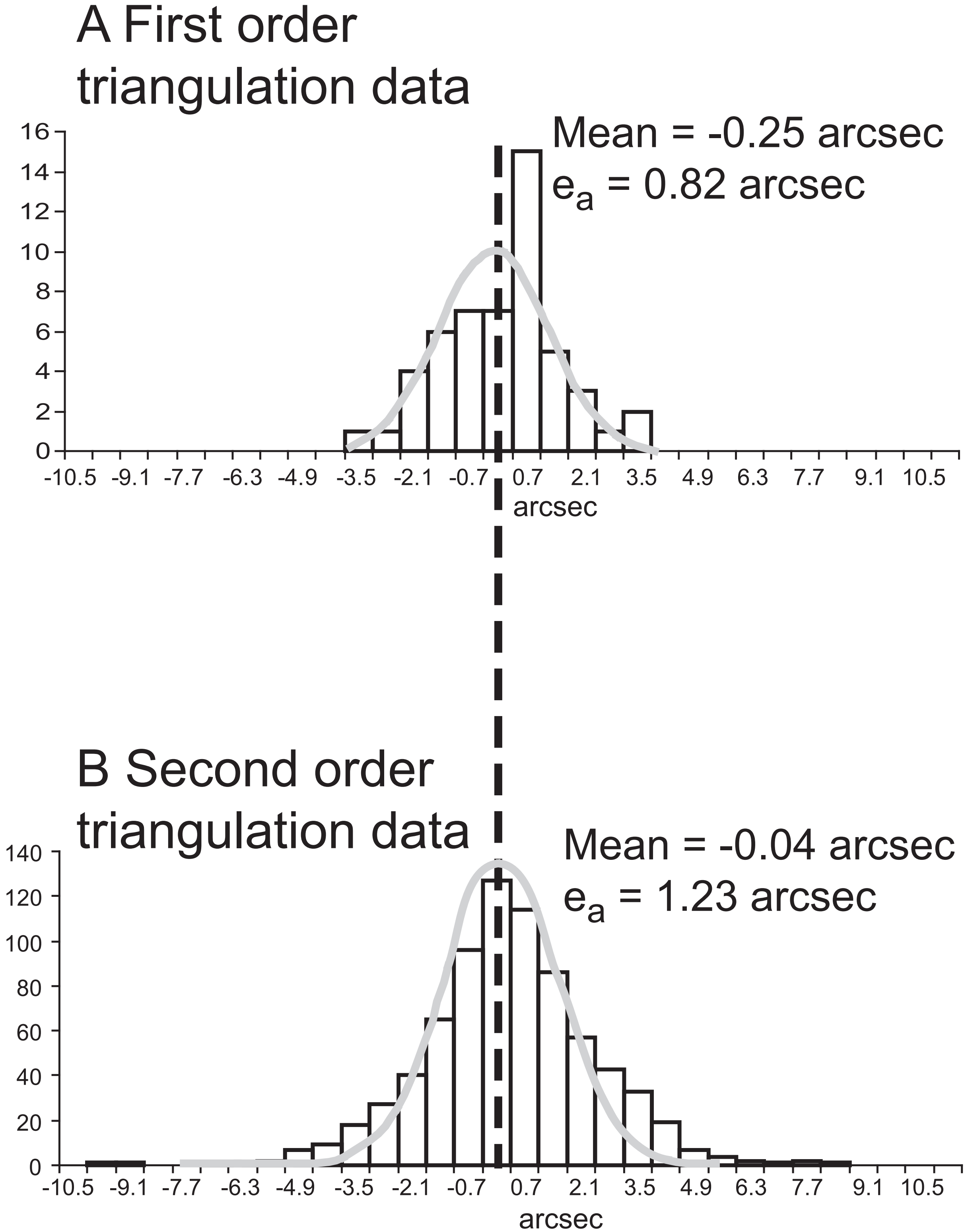

Figure 4. Results of the error analysis of the triangulation data (see also Table 1). Solid line shows Gaussian curve fit to the data. (A) Frequency distribution of the first order triangle closures (equation 1). ϵ_a indicates the average observational error computed with equation 2; (B) Same as (A) for second order triangulation data.

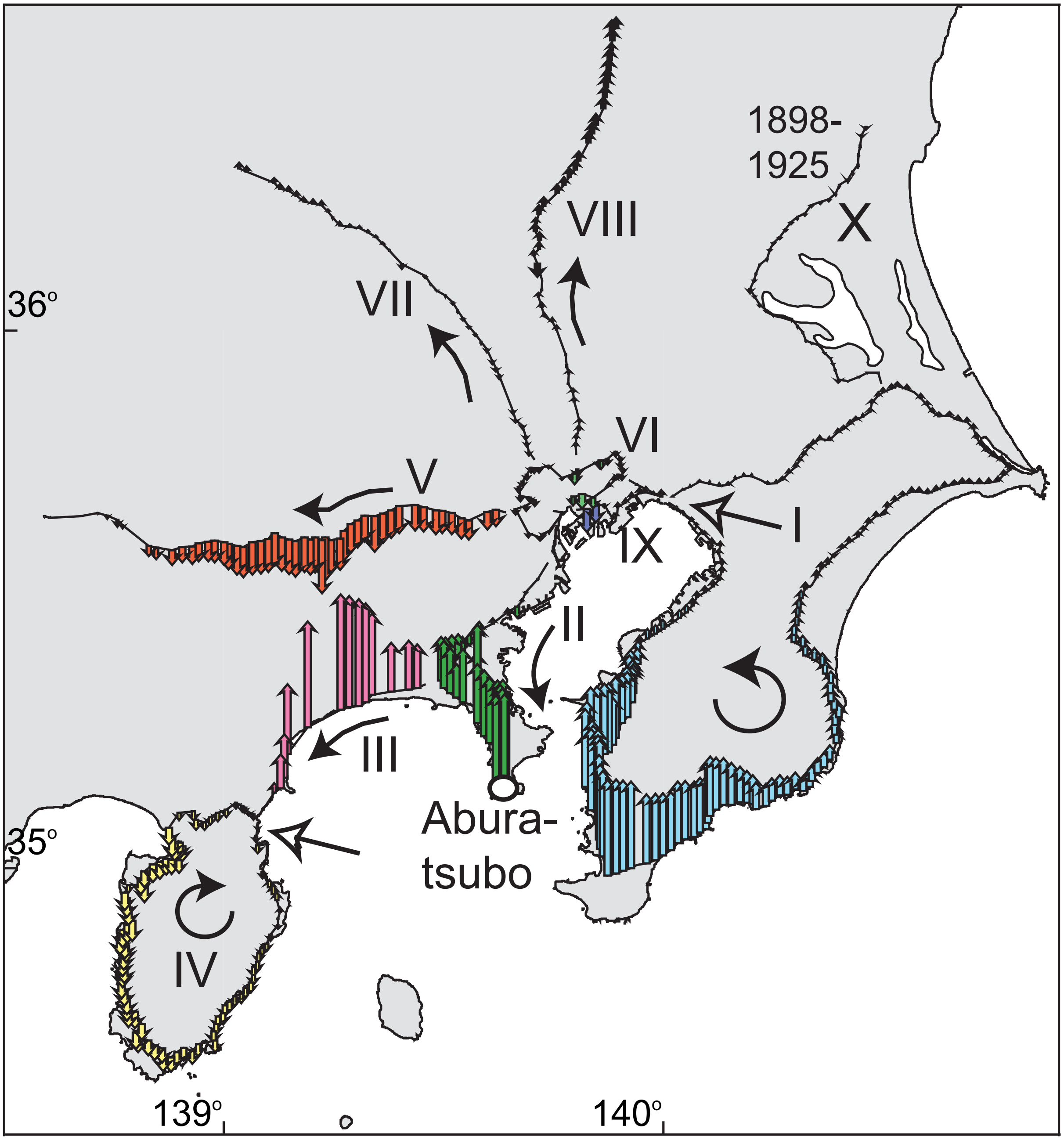

Figure 5. Leveling routes in Kanto and the vertical displacement derived from surveys before and shortly after 1923. The oval indicates tide gage station Aburatsubo that provides the data for the absolute vertical reference frame. The roman enumeration and color coding of the arrows correspond to the profiles shown in Figure 10. The direction in which the profiles in Figure 10 display displacement along the routes is here indicated by a black arrow. For closed loops I and IV the white arrow indicates the start of the profile.

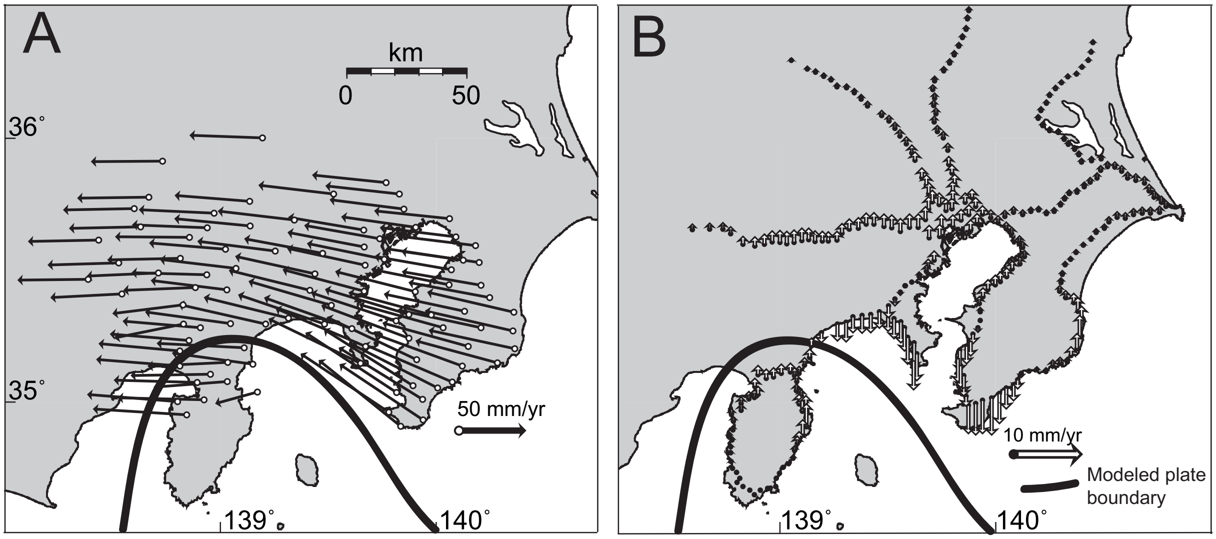

Figure 6. The interseismic velocity field from *Nishimura and Sagiya* [2004] relative to fixed Eurasia. The model is based on continuous GPS data between 1995 and 2000 and produces a velocity field that consists of a rigid plate component and elastic effects caused by the interseismic locking of plates along their interfaces within the boundary zones. A plate interface is parameterized by a multirectangular fault system which accommodates backslip. (A) Horizontal velocity vectors plotted at a selection of the first and second order triangulation bench marks used in this study; (B) Vertical velocities plotted at selected leveling benchmarks.

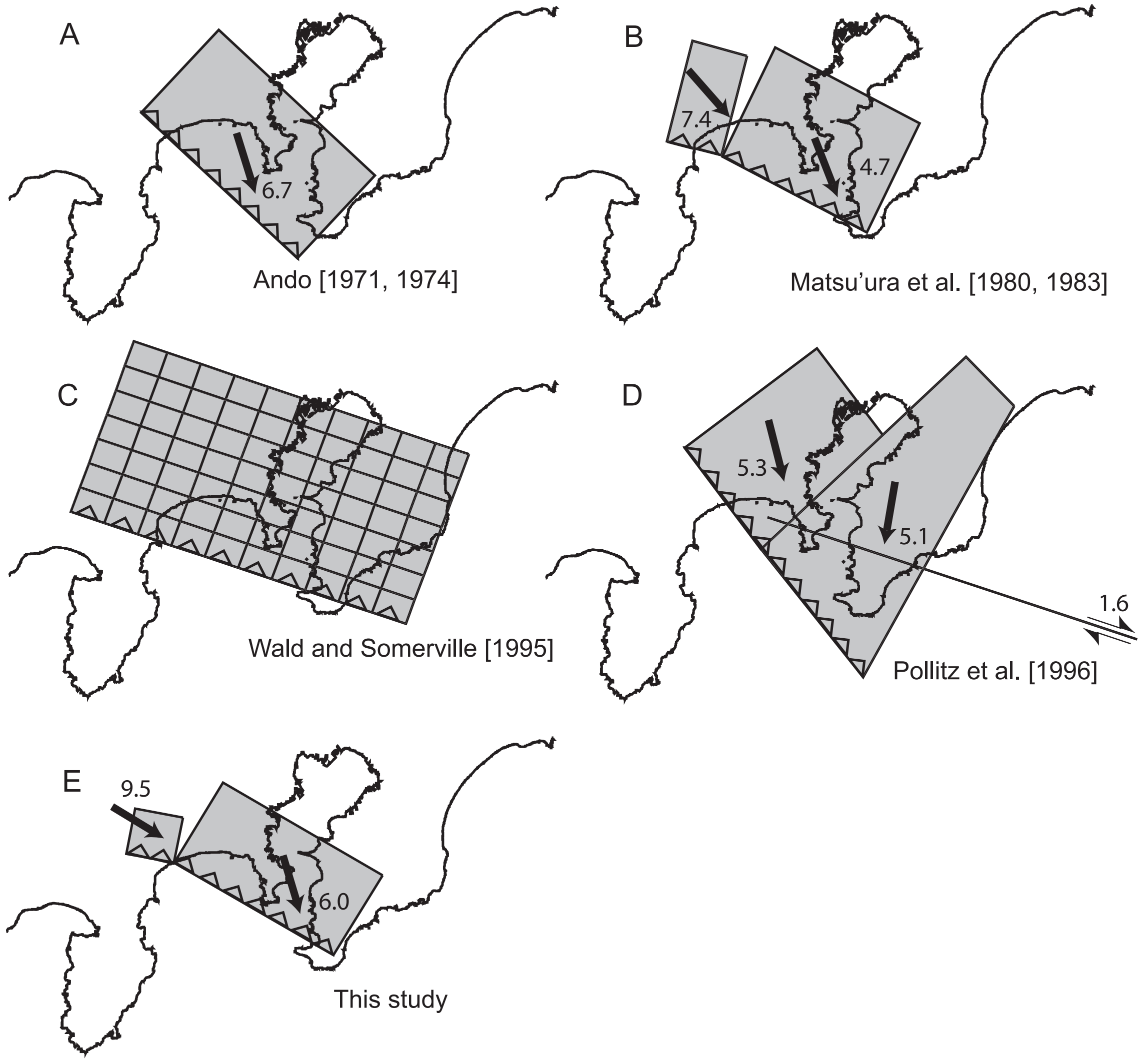

Figure 7. Surface projection of a selection of fault plane models that are based on historical geodetic observations (triangulation and leveling data). The arrows indicate the slip direction, the numbers the magnitude of the slip for the uniform slip models.

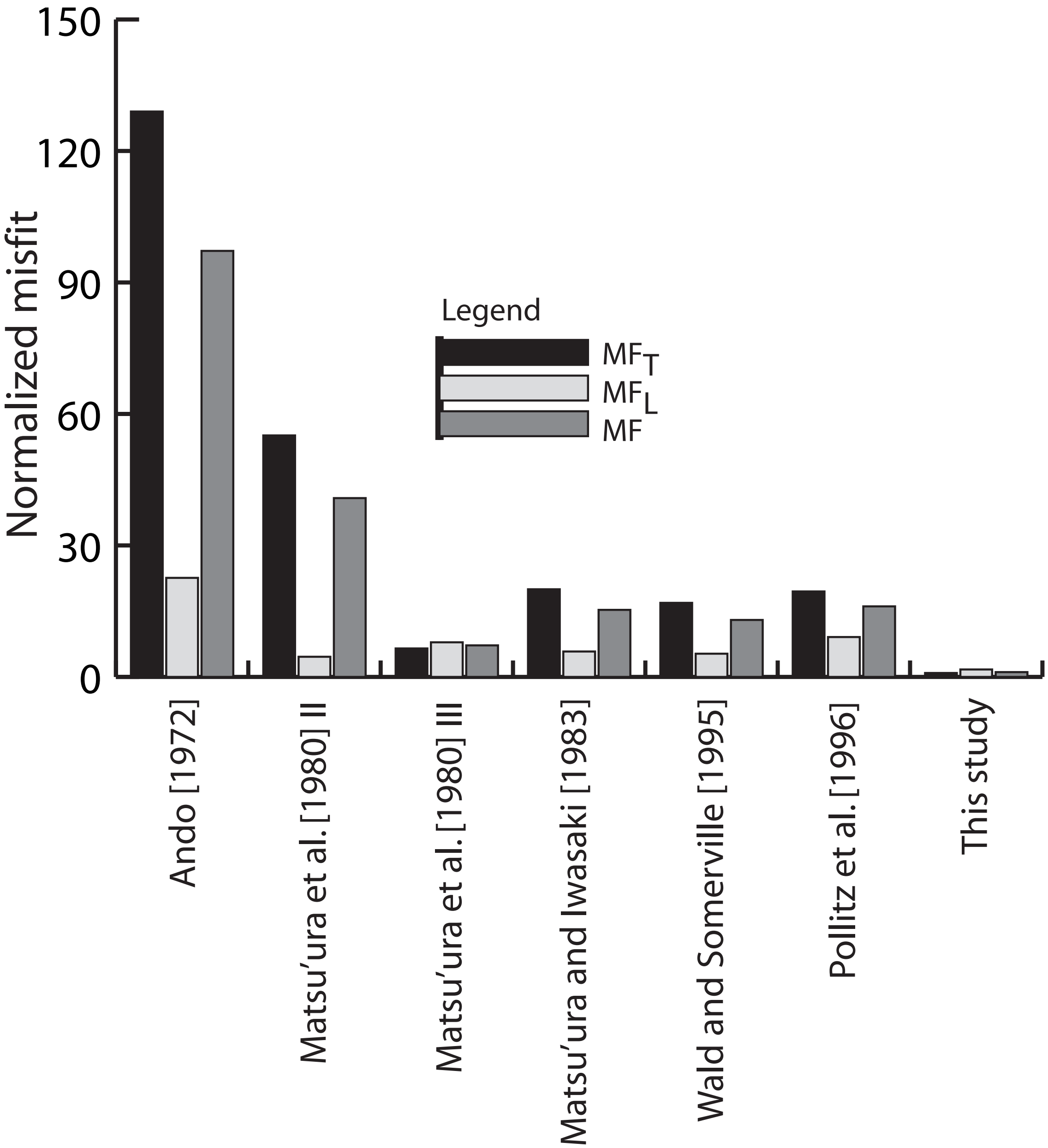

Figure 8. Histogram of normalized root-mean-square (NRMS) misfit values for a selection of fault plane models that are based on historical geodetic observations. MF$_T$ normalized root mean-square (NRMS) misfit (equation 3) between model and triangulation data; MF$_L$ NRMS misfit between model and leveling data; MF NRMS misfit between model and all data.

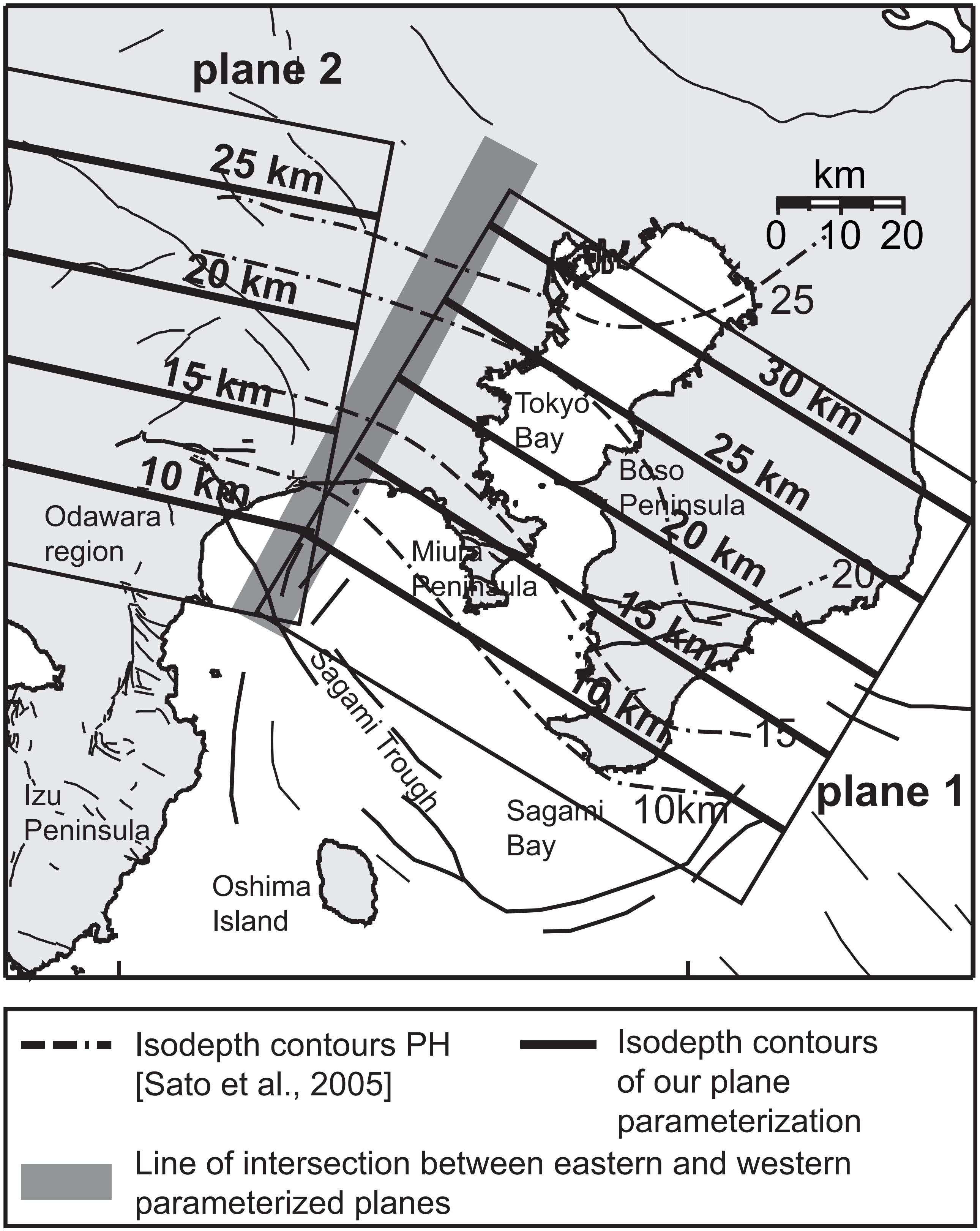

Figure 9. Planar two-segment parametrization of the image of the PH plate interface as presented by the seismic reflection study by *Sato et al.* [2005].

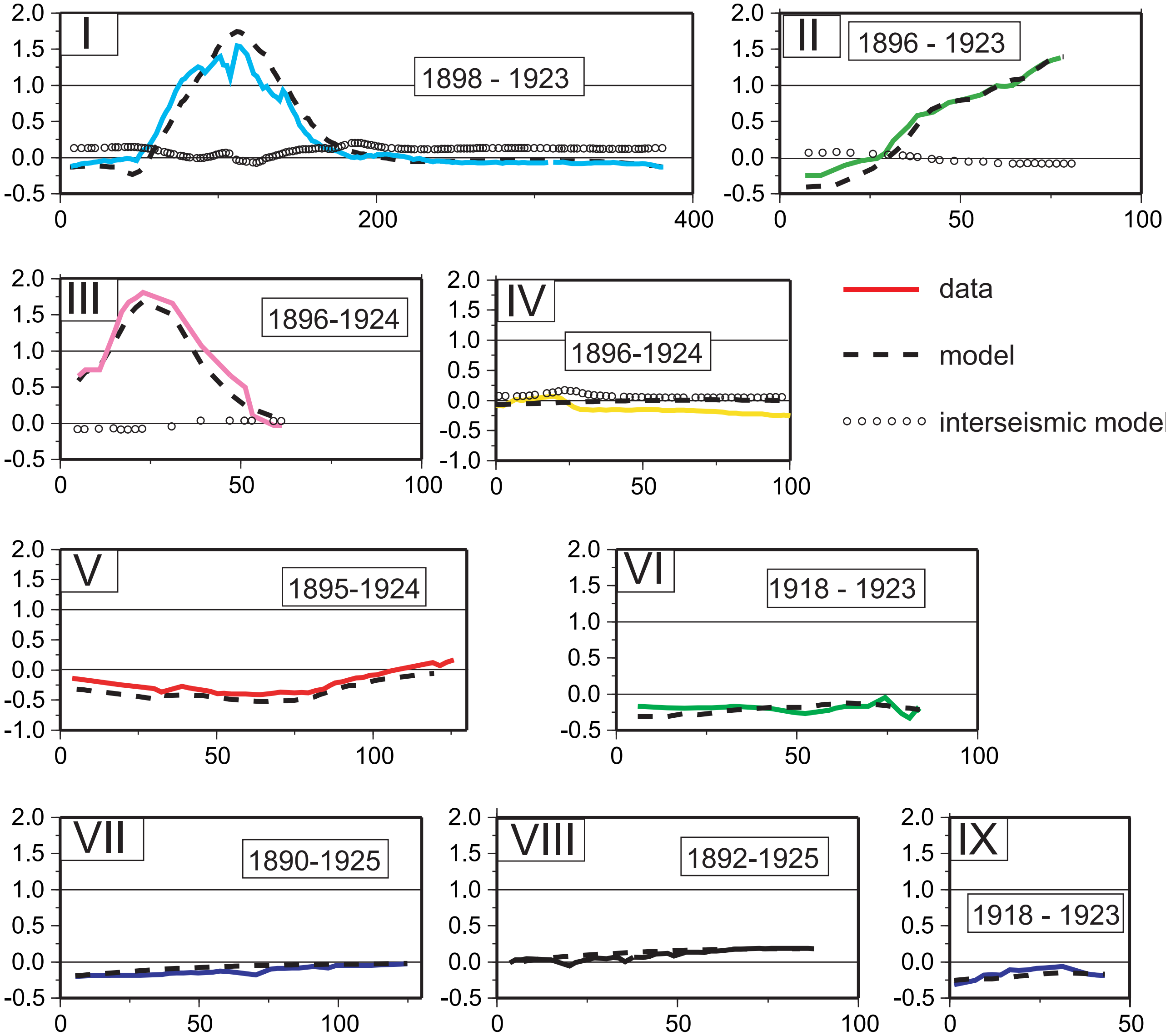

Figure 10. Fit of our uniform source models to the leveling observations that are adjusted for interseismic deformation and indicated by the colored lines. The black lines represent the absolute vertical displacement of our model. The color coding and roman numerals correspond to the level routes shown in Figure 5. The vertical component of the interseismic deformation field, plotted for routes I through IV, is omitted for routes V through IX, because there its signal is indistinguishable from zero displacement. Route X (Figure 5) is not displayed here, because the observations do not show any deformation and both models predict zero vertical displacement along this route. The two-plane model curves are not shown for routes II, IV, VI through X, because they are almost identical to the single-plane curves.

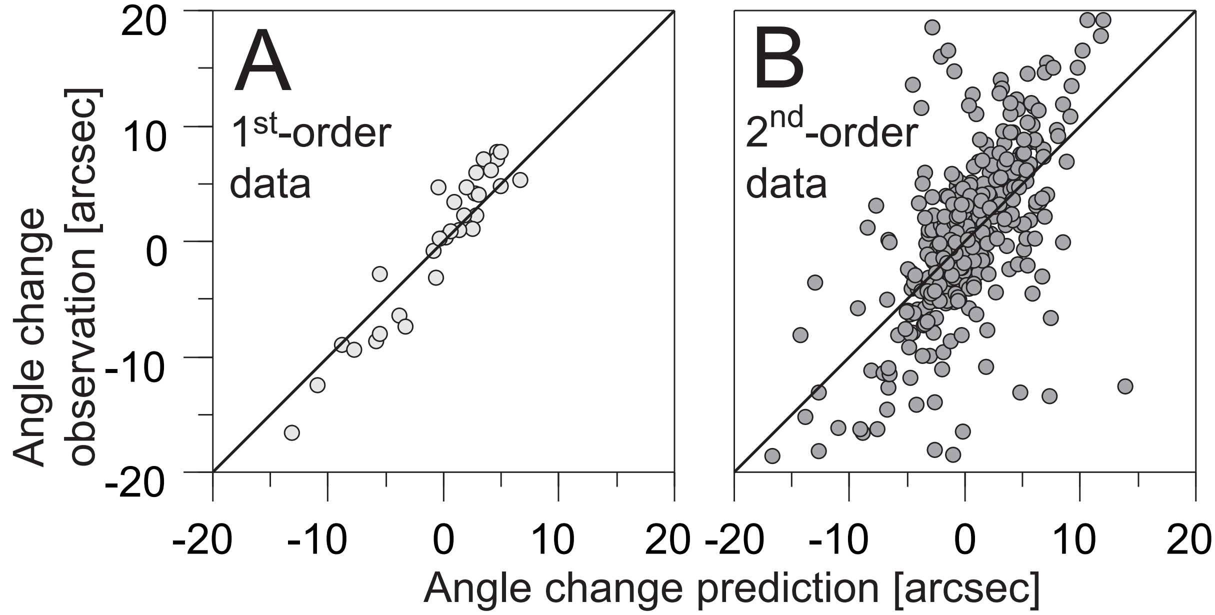

Figure 11. Correlation between model predictions and first order (A) and second order (B) observations.

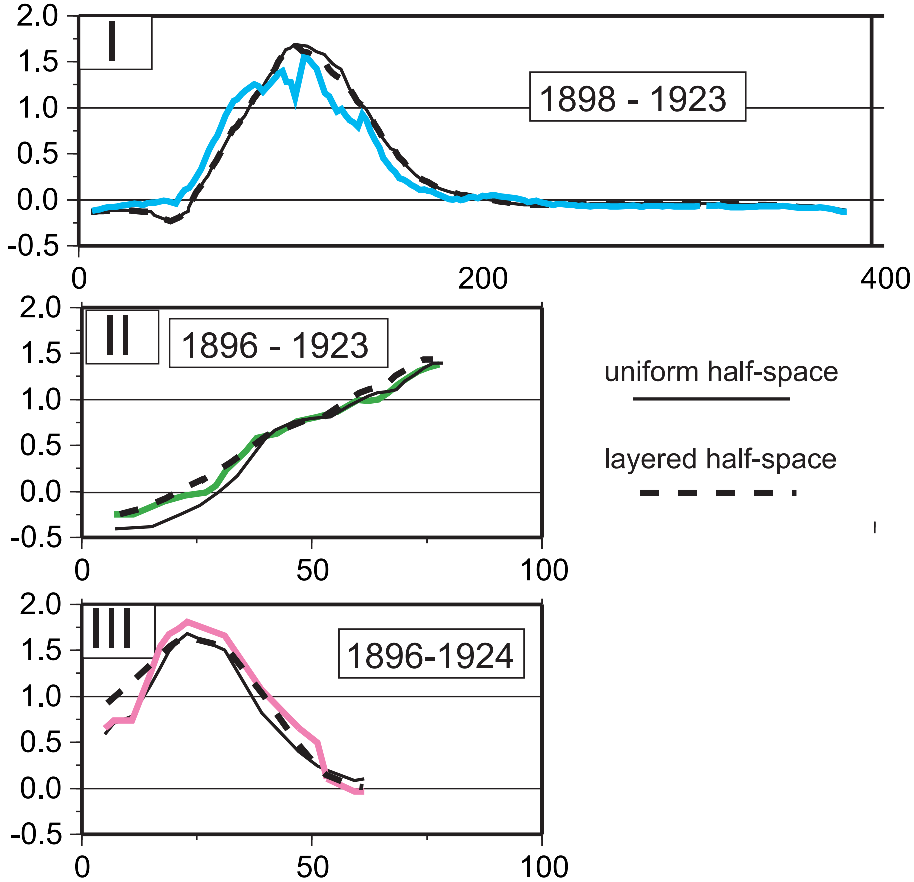

Figure 12. Difference in data fit between the preferred source model in a homogenous half-space and in a layered Earth (Table 5). (A) Only the fit to the leveling data along routes I, II and III changes significantly; (B) Absolute difference in angle change predictions.

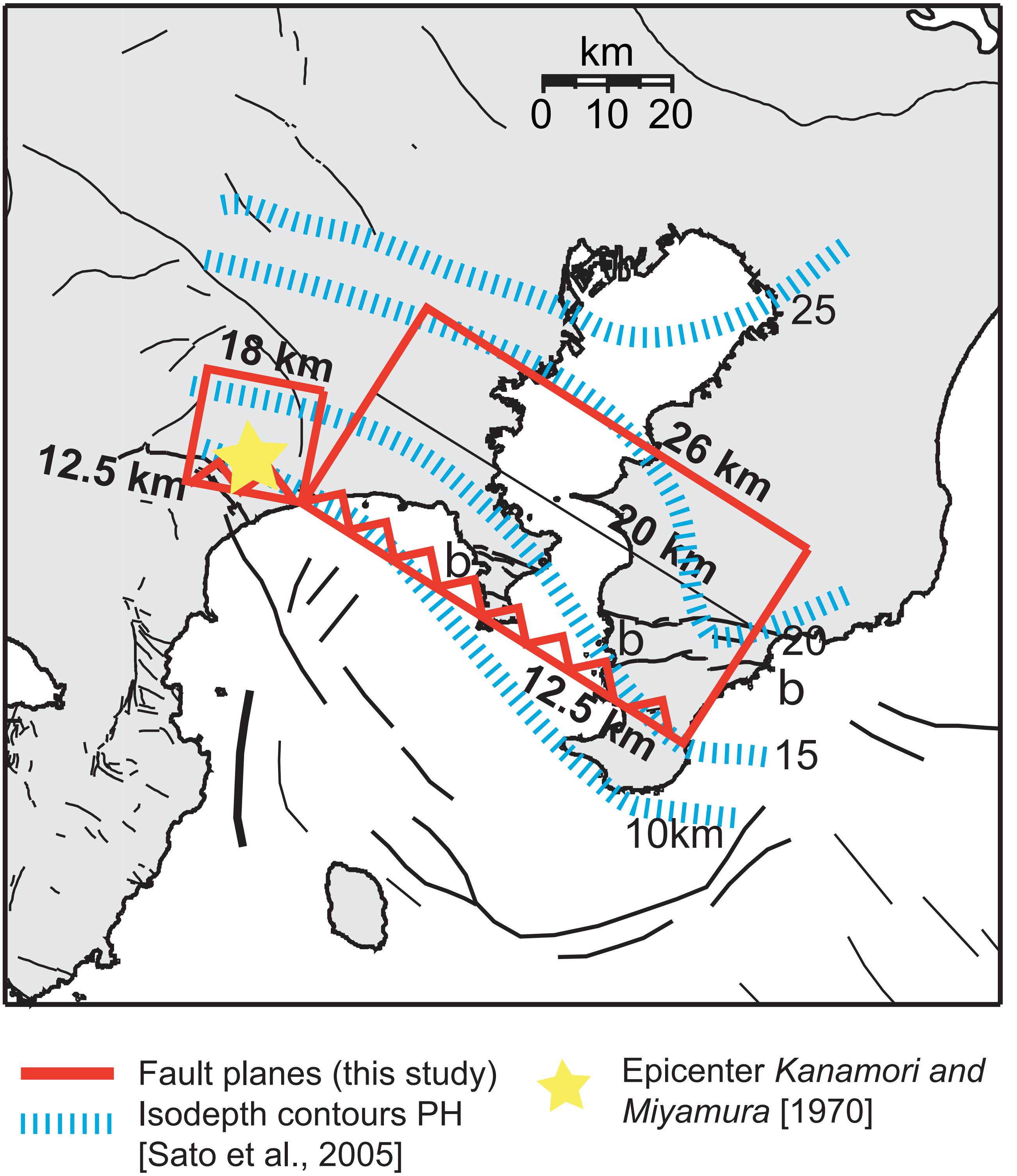

Figure 13. Our two-plane uniform slip source model with isodepth contours for both planes and isodepth contours of the Philippine Sea plate after *Sato et al.* [2005].

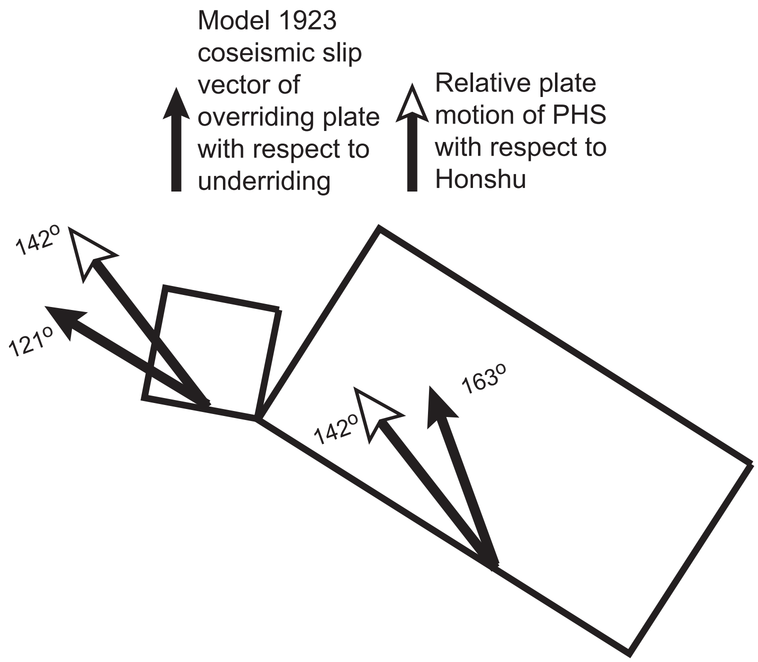

Figure 14. Relative plate motion orientation (an average of the four different plate motion models shown in Figure 15) and resolved slip on the double fault plane model.

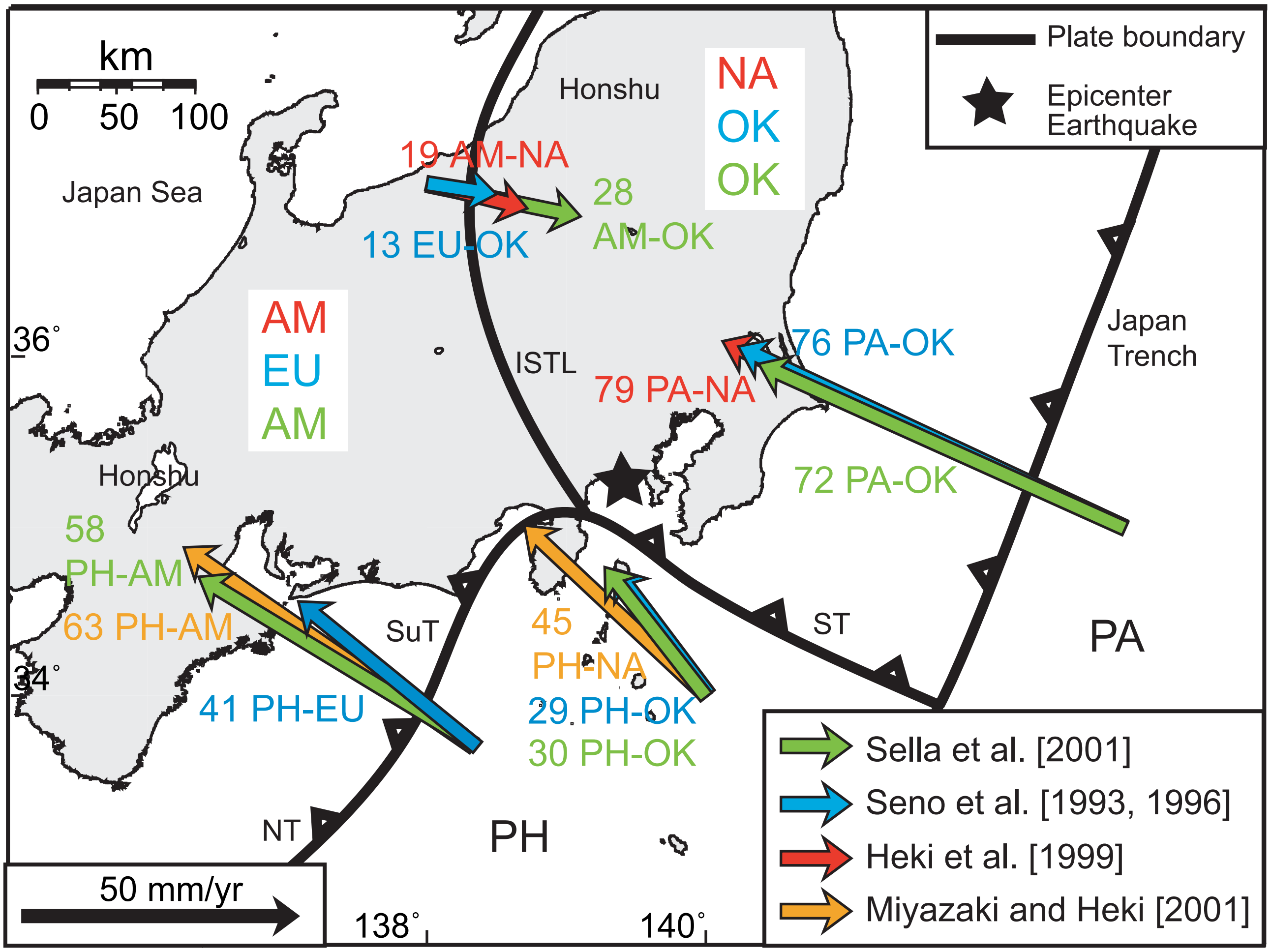

Figure 15. Plate tectonic models for central Japan based on GPS velocity data. Key: AM Amurian, EU Eurasian, NA North American, OK Okhotsk, PA Pacific, PH Philippine Sea plates; ISTL Itoigawa-Shizuoka Tectonic Line, NT Nankai Trough, ST Sagami Trough, SuT Suruga Trough. Arrows show the plate velocities with respect to northern Honshu. Numbers indicate plate velocities in mm/yr, the colors correspond to the colors of the arrows. Velocities shown are the rates predicted by the three main plate models for Japan. In the plate model of *Heki et al.* [1999] and *Heki and Miyazaki* [2001] central and western Honshu are located on the Amurian plate that encompasses eastern Asia and moves independently from the Eurasian plate. This model can explain the regional relative plate motion without the necessity to distinguish the Okhotsk plate from the North American plate. Seno et al. [1993, 1996] postulate the existence of the Okhotsk plate separated from the North American plate along a boundary in Siberia. In this model northeastern Honshu is on the Okhotsk plate and southwestern Honshu is considered as part of Eurasia. *Sella et al.* [2002] use both the Okhotsk and the Amurian

Table 1. Error analysis of the triangulation surveys between 1883 and 1931.

id	Period	Stations *	Closures	δc_{max} ‡ [arcsec]	ϵ_a £ [arcsec]
		first order network			
a	1891-1898	46	44	3.55	0.83
b	1924-1931	37	11	3.06	0.79
a and b	1891-1931	60	55	3.55	0.82
		second order network			
c	1883-1902	1097	694	-10.50	1.23
d	1925-1931	145	79	6.43	1.31
c and d	1883-1931	1136	773	-10.50	1.23

* Number of stations that contributes to closures

¶ Signal-to-noise ratio

‡ Largest closure (equation 1) found in the particular data subset.

£ Average observation error (equation 2).

Table 2. Components of the geodetic data set used in this study.

Bench marks	Data	Preseismic survey	Postseismic survey	SNR ¶
		1^{st} order triangulation		
15	31	1891-1898	1924-1925	7.86
		2^{nd} order triangulation		
178	435	1883-1900	1924-1925	5.67
		1^{st} and 2^{nd} order triangulation combined		
193	466	1883-1900	1924-1925	5.88
		leveling		
469	469	1898-1918	1923-1925	43.78

¶ Signal-to-noise ratio

Table 3. Estimates of leveling errors averaged over periods 1884-1923 and 1923-40.

Year	1884	'92	'95	'98	1902	'09	'18	'24	'25	'29	'30	'34	'37	'38	'42
#[†]	77	56	54	63	60	51	73	213	40	44	58	40	118	152	76
α [mm/km] [§]	1.55	0.61	0.60	0.50	0.53	0.55	0.46	0.63	0.53	0.53	0.50	0.69	0.56	0.72	0.63
$\widetilde{\alpha}$ [mm/km] [‡]	1.55	0.54						0.62							

[†] Number of randomly chosen double-run leveling sections that contribute to α.

[§] Observed average leveling error per year normalized to a distance of 1 km.

[‡] Assigned average leveling error per multiple year period normalized to a distance of 1 km.

Table 4. Comparison of source models of the 1923 Kanto earthquake, based on geodetic data.

Strike[a]	Dip	Rake	Length[b] [km]	Width[c] [km]	Lon[d]	Lat[d]	Depth[e] [km]	Slip[f] [m]	Slip azimuth[g]	MF_T[h]	MF_L[i]	MF[j]	dof
						Ando [1974]							
-45°	30°	153°	85	55	140.1°E	35.1°N	0.0	6.7	162°	22.6	129.9	97.2	9
						Matsu'ura et al. [1980], *model II*							
-66°	25°	140°	95	54	140.1°E	35.3°N	1.9	4.8	154°	4.6	55.1	40.8	9
						Matsu'ura et al. [1980], *model III*							
-64°	23°	138°	63	55	140.1°E	35.3°N	1.5	4.7	158°	7.9	6.5	7.2	15
-75°	26°	147°	22	45	139.4°E	35.5°N	1.5	7.4	138°				
						Matsu'ura and Iwasaki [1983]							
-67°	26°	142°	93	53	140.1°E	35.3°N	2	4.6	151°	5.8	20.0	15.3	9
						Wald and Somerville [1995]							
-70°	25°	90-180°[l]	130	70	139.5°E [m]	35.0°N [m]	2.0	0-7.8[n]	110°-200°[o]	6.1	16.2	12.5	140
						Pollitz et al. [1996]							
-39°	38°	156°	41	74	139.9°E	35.4°N	0.3	5.3	165°	9.1	19.5	16.1	25
-68°	90°	180°	130	12	140.8°E	35.8°N	0.3	1.6	112°				
-39°	20°	132°	75[p]	116	140.5°E	35.5°N	0.3	5.1	189°				
						This study, best fit to leveling data							
-59°[q]	20°[q]	138°	71[r]	43	140.13°E	35.28°N	12.8[r]	6.0	163°	3.9	0.9	1.4	9
-79°[q]	17°[q]	160°	23	21	139.27°E[r]	35.46°N[r]	12.8[r]	9.5	121°				

Table 5. Velocity structure model for Kanto from *Takeo and Kanamori* [1992].

Depth[a] (km)	Thickness (km)	V_p (km/sec)	V_s (km/sec)	ρ (g/cc)
0.0[b]	*1.0*[b]	*1.83*[b]	*0.7*[b]	*2.0*[b]
1.0	1.7	2.8	1.3	2.3
2.7	3.4	5.6	2.9	2.5
6.1	12.9	6.0	3.4	2.6
19.0	-	6.8	4.0	3.0

[a] Depth to the top of the layer.

[b] The soft sedimentary layer characteristic for the Kanto plain.